Available online at www.sciencedirect.com
SCIENCE DIRECT®
ELSEVIER
International Journal of Solids and Structures 41 (2004) 7209–7240
INTERNATIONAL JOURNAL OF SOLIDS and STRUCTURES
www.elsevier.com/locate/ijsolstr

Nonlocal microplane model with strain-softening yield limits

Zdeněk P. Bažant [a,*], Giovanni Di Luzio [b,*]

[a] McCormick School of Engineering and Applied Science, Northwestern University, CEE, 2145 Sheridan Road, Evanston, IL 60208-3109, USA
[b] Department of Structural Engineering, Politecnico di Milano, Piazza Leonardo da Vinci 32, 20133 Milan, Italy

Received 14 November 2002; received in revised form 26 May 2004
Available online 20 July 2004

Abstract

The paper deals with the problem of nonlocal generalization of constitutive models such as microplane model M4 for concrete, in which the yield limits, called stress–strain boundaries, are softening functions of the total strain. Such constitutive models call for a different nonlocal generalization than those for continuum damage mechanics, in which the total strain is reversible, or for plasticity, in which there is no memory of the initial state. In the proposed nonlocal formulation, the softening yield limit is a function of the spatially averaged nonlocal strains rather than the local strains, while the elastic strains are local. It is demonstrated analytically as well numerically that, with the proposed nonlocal model, the tensile stress across the strain localization band at very large strain does soften to zero and the cracking band retains a finite width even at very large tensile strain across the band only if one adopts an ''over-nonlocal'' generalization of the type proposed by Vermeer and Brinkgreve [In: Chambon, R., Desrues, J., Vardoulakis, I. (Eds.), Localisation and Bifurcation Theory for Soils and Rocks, Balkema, Rotterdam, 1994, p. 89] (and also used by Planas et al. [Basic issue of nonlocal models: uniaxial modeling, Tecnical Report 96-jp03, Departamento de Ciencia de Materiales, Universidad Politecnica de Madrid, Madrid, Spain, 1996], and by Strömberg and Ristinmaa [Comput. Meth. Appl. Mech. Eng. 136 (1996) 127]). Numerical finite element studies document the avoidance of spurious mesh sensitivity and mesh orientation bias, and demonstrate objectivity and size effect.

Keywords: Microplane model; Concrete; Nonlocal continuum; Fracture; Damage; Quasibrittle materials; Softening; Numerical methods; Finite elements

1. Introduction

Since its inception almost two decades ago (Bažant, 1984; Bažant et al., 1984), the nonlocal continuum approach to distributed softening damage has generally been accepted as the proper way to avoid spurious excessive localization and ensure mesh-independent energy dissipation (Bažant and Jirásek, 2002). The nonlocal models generally work well for the initial post-peak damage, which usually suffices for capturing

* Corresponding authors. Tel.: +1-847-491-4025 (Z.P. Bažant), Tel.: +39-022-399-4278; fax: +39-022-399-4220 (G. Di Luzio).
E-mail addresses: z-bazant@northwestern.edu (Z.P. Bažant), diluzio@stru.polimi.it (G. Di Luzio).

0020-7683/$ - see front matter © 2004 Elsevier Ltd. All rights reserved.
doi:10.1016/j.ijsolstr.2004.05.065

the size effect on structural strength. However, unlike the nonlocal continuum damage model (Pijaudier-Cabot and Bažant, 1987; Bažant and Pijaudier-Cabot, 1988), the plasticity-based models with softening yield limit (initiated by Bažant and Lin, 1988b) are unable to simulate properly the far post-peak response (Bažant and Jirásek, 2002; Jirásek and Rolshoven, 2003; Rolshoven and Jirásek, 2001). In particular, depending on the plasticity model formulation, it has been proven difficult to simulate the vanishing of stress at large tensile strain across a damage band, while, for some other plasticity model, at very large strains, the damage band was shown to localize to zero width. This is a serious problem for dynamic behavior because the energy absorption capability of the structure with its size dependence is not captured correctly.

To remedy this problem with nonlocal softening plasticity-based models, Vermeer and Brinkgreve (1994), Planas et al. (1996) and Strömberg and Ristinmaa (1996) proposed a novel formulation which we will call "over-nonlocal". In their formulation, the nonlocal variable is enlarged by a factor m larger than 1, and then reduced by the $(m-1)$-multiple of the corresponding local variable. They demonstrated this approach for relatively simple tensorial constitutive models of isotropic softening-plasticity.

This study will address the problem of the far post-peak nonlocality for a damage-constitutive model of the microplane type, and in particular for its recent powerful version for concrete called model M4 (Bažant et al., 2000; Caner and Bažant, 2000). Aside from the over-nonlocal aspect of the formulation, an alternative new approach to far post-peak behavior will be proposed. It will exploit the fact that, in model M4, the strain-softening behavior is completely characterized by strain-dependent yield limits (called the stress–strain boundaries). It will be shown that the easiest way to achieve a satisfactory far post-peak behavior, with a vanishing tensile stress across the damage band, is to make these limits functions on the nonlocal strain instead of the local strain. This makes it possible to simulate the transition to complete fracture.

Quasibrittle materials, such as concrete, rocks, ceramics, sea ice, and fiber composites, exhibit distributed cracking and other softening damage which needs to be described as a strain softening continuum. Already in the mid-1970s (Bažant, 1976) it was recognized that the concept of softening continuum damage leads to serious problems (Bažant and Jirásek, 2002)—the boundary value problem becomes ill-posed and the numerical calculations cease to be objective, exhibiting pathological spurious mesh sensitivity and unrealistic damage localization as the mesh is refined. To suppress it and to prevent the damage from localizing into a zone of zero volume, the continuum theory must be complemented by certain conditions called 'localization limiters', involving a characteristic length of the material (Bažant, 1976; Bažant and Oh, 1983; Bažant et al., 1984; Bažant and Belytschko, 1985).

As the simplest localization limiter, one may adjust the post-peak slope of the stress–strain diagram as a function of the element size. This is done in the crack band model (Bažant, 1976; Bažant and Oh, 1983), which is the model most widely used in practice and adopted in commercial codes (DIANA, ATENA, SBETA, etc.). Another popular regularizing technique uses a second-order gradient model (Aifantis, 1984; Zbib and Aifantis, 1988; Lasry and Belytschko, 1988; Mühlhaus and Aifantis, 1991; de Borst and Mühlhaus, 1992a,b; Vardoulakis and Aifantis, 1991; Pamin, 1994). Recently, an effective modification of the gradient approach has been developed by Peerlings et al. (1996). A different gradient-type regularization model is based on the concept of Cosserat continuum (Cosserat and Cosserat, 1909), which is able to limit localization in a shear band but not in tension (Mühlhaus and Vardoulakis, 1987; de Borst, 1991; Steinmann and Willam, 1992). A simple regularization technique, which works only for a limited range of loading rates, is the viscoplastic regularization, in which some artificial strain-rate dependent terms are inserted into the constitutive law (Needleman, 1988; Loret and Prevost, 1990).

A broad class of localization limiters is based on the concept of a *nonlocal continuum*, which is used in this work. The nonlocal concept was introduced in the 1960s (Eringen, 1966; Kröner, 1968; etc.) for elastic deformations and later expanded to hardening plasticity. In a nonlocal continuum, the stress at a certain point depends not only on the strain at that point itself but also on the strain field in the neighborhood of that point. Bažant (1984) and Bažant et al. (1984) introduced the nonlocal concept as a localization limiter

for a strain-softening material. This formulation was soon improved in the form of the nonlocal damage theory (Pijaudier-Cabot and Bažant, 1987; Bažant and Pijaudier-Cabot, 1988), nonlocal plasticity with a softening yield limit (Bažant and Lin, 1989) and nonlocal smeared cracking (Bažant and Lin, 1988b), and was demonstrated in practical problems (Bažant and Lin, 1988a, 1989; Saouridis and Mazars, 1992).

The governing parameter in the nonlocal continuum is the material characteristic length l depending on the size of the neighborhood over which the strain or some other variable is averaged. When l is equal to or less than the element size, the nonlocal formulation reduces to a local formulation. The characteristic length has a major influence on the softening behavior of structure. In the early studies, this length was assumed to be correlated to the maximum aggregate size d_a, $l = 3d_a$ (Bažant and Oh, 1983). However, it is now accepted that the characteristic length l is also influenced by other parameters (especially Irwin's characteristic size of the fracture process zone). Experience shows that the optimum value of l can change significantly from one type of problem to another, which could be explained by the fact that the directional dependence of microcrack interactions (Bažant, 1994; Ožbolt and Bažant, 1996) is ignored.

Classically, the nonlocal approach has been applied to the standard constitutive models expressed in terms of the stress and strain tensors and their invariants. During the last decade, the earlier nonlocal approach has been introduced into an early version of the microplane model (Bažant and Ožbolt, 1990; Ožbolt and Bažant, 1996), in which the constitutive behavior is characterized in terms of stress and strain vectors acting on arbitrarily oriented planes in the material (Bažant, 1984; Bažant and Oh, 1985). The objective of this paper is to combine the microplane model with the recently improved nonlocal approach that leads to a correct localization behavior, and demonstrate it for a recent version of microplane model employing the concept of softening stress–strain boundaries. Although the main advantage of microplane model lies in the simulation of damage for complex compressive triaxial stress histories, the comparisons with experiments will have to focus on tensile fracture because there are hardly any test data on damage localization for such histories.

2. Review of microplane model

The microplane constitutive model is defined by a relation between the stresses and strains acting on a plane in the material called the microplane, having an arbitrary orientation (characterized by its unit normal n_i). The basic hypothesis, which enhances stability of post-peak strain softening (Bažant, 1984), is the kinematic constraint, consisting in the fact that the strain vector $\overrightarrow{\epsilon_N}$ on the microplane (Fig. 1a) is the projection of the strain tensor $\boldsymbol{\epsilon}$, i.e., $\epsilon_{Ni} = \epsilon_{ij} n_j$. The normal strain on the microplane is $\epsilon_N = n_i \epsilon_{Ni}$, that is,

$$\epsilon_N = N_{ij} \epsilon_{ij}, \tag{1}$$

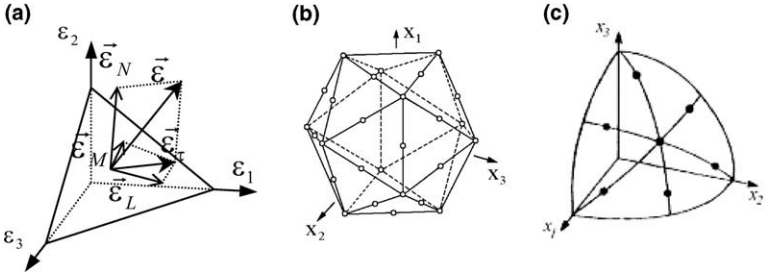

Fig. 1. (a) Strain components on general microplane; (b) directions of microplane normals (circles) for system of 21 microplanes per hemisphere; (c) directions of microplane normals (circles) for system of 28 microplanes per hemisphere.

where $N_{ij} = n_i n_j$ (and the repetition of the subscripts, referring to Cartesian coordinates x_i, implies summation over $i = 1, 2, 3$). The shear strains on each microplane are characterized by their components in chosen directions M and L given by orthogonal unit coordinate vectors $\vec{m}$ and $\vec{l}$, of components m_i, l_i, lying within the microplane. The unit coordinate $\vec{m}$ is chosen and $\vec{l}$ is obtained as $\vec{l} = \vec{m} \times \vec{n}$. To minimize directional bias, vectors $\vec{m}$ are alternatively chosen normal to axes x_1, x_2, or x_3. The shear strain components in the directions of $\vec{m}$ and $\vec{l}$ are $\epsilon_M = m_i(\epsilon_{ij} n_j)$ and $\epsilon_L = l_i(\epsilon_{ij} n_j)$, and by virtue of the symmetry of tensor ϵ_{ij},

$$\epsilon_M = M_{ij}\epsilon_{ij}, \qquad \epsilon_L = L_{ij}\epsilon_{ij}, \tag{2}$$

in which $M_{ij} = (m_i n_j + m_j n_i)/2$ and $L_{ij} = (l_i n_j + l_j n_i)/2$ (Bažant and Prat, 1988).

Because of the kinematic constraint relating the strains on the microlevel (microplane) and macrolevel (continuum), the static equivalence (or equilibrium) of stresses between the macro- and microlevels is expressed by the principle of virtual work (Bažant, 1984), written for the surface Ω of a unit hemisphere:

$$\frac{2\pi}{3}\sigma_{ij}\delta\epsilon_{ij} = \int_\Omega (\sigma_N \delta\epsilon_N + \sigma_L \delta\epsilon_L + \sigma_M \delta\epsilon_M)\,\mathrm{d}\Omega. \tag{3}$$

This equation means that the virtual work of macrostresses (continuum stresses) within a unit sphere must be equal to the virtual work of microstresses (microplane stress components) regarded as the tractions on the surface of a sphere (for a detailed physical justification, see Bažant et al., 1996a). The integral physically represents a homogenization of different contributions coming from planes of various orientations within the material. Substituting $\delta\epsilon_N = N_{ij}\delta\epsilon_{ij}$, $\delta\epsilon_L = L_{ij}\delta\epsilon_{ij}$ and $\delta\epsilon_M = M_{ij}\delta\epsilon_{ij}$, and noting that the last variational equation must hold for any variation $\delta\epsilon_{ij}$, one gets the following basic equilibrium relation (Bažant, 1984):

$$\sigma_{ij} = \frac{3}{2\pi}\int_\Omega s_{ij}\,\mathrm{d}\Omega = 6\sum_{\mu=1}^{N_m} w_\mu s_{ij}^{(\mu)} \quad \text{with } s_{ij} = \sigma_N N_{ij} + \sigma_L L_{ij} + \sigma_M M_{ij}. \tag{4}$$

The numerical integration, indicated above, is best done according to an optimal Gaussian integration formula for a spherical surface (Stroud, 1971; Bažant and Oh, 1986) representing a weighted sum over the microplanes of orientations $\vec{n}_\mu$, with weights w_μ normalized so that $\sum_{\mu=1}^{N_m} w_\mu = 1/2$ (Bažant and Oh, 1985, 1986). An efficient formula that still yields acceptable accuracy involves 21 microplanes (Bažant and Oh, 1986; Fig. 1b); in this work the Stroud's formula with 28 microplanes has been used (Fig. 1c). In finite element programs, integral (4) must be evaluated at each integration point of each finite element in each time step. The values of $N_{ij}^{(\mu)}$, $M_{ij}^{(\mu)}$ and $L_{ij}^{(\mu)}$ for all the microplanes $\mu = 1, \ldots, N$ are common to all integration points of all finite elements, and are calculated and stored in advance.

The most general constitutive relation on the microplane level may give σ_N, σ_L and σ_M as functionals of the histories of ϵ_N, ϵ_M, ϵ_L. But normally it is suffices to consider that each of σ_N, σ_L and σ_M depends only on its current corresponding strain ϵ_N, ϵ_M, ϵ_L because cross dependencies on the macrolevel, such as shear dilatancy, are automatically captured by interaction among microplanes of various orientations. An exception is the frictional yield condition relating the normal and the shear components on the microplane with no strain dependence.

In microplane model M4 (as well as M3, Bažant et al., 1996a,b and M5, Bažant and Caner, 2002), the constitutive relation in each microplane is defined by (1) incremental elastic relation and (2) stress–strain boundaries (softening yield limits) that cannot be exceeded. The normal components are split into their normal and deviatoric parts, i.e. $\sigma_N = \sigma_V + \sigma_D$, $\epsilon_N = \epsilon_V + \epsilon_D$, and then the incremental elastic relations are written as

$$\mathrm{d}\sigma_V = E_V \mathrm{d}\epsilon_V, \qquad \mathrm{d}\sigma_D = E_D \mathrm{d}\epsilon_D, \qquad \mathrm{d}\sigma_M = E_T \mathrm{d}\epsilon_M, \qquad \mathrm{d}\sigma_L = E_T \mathrm{d}\epsilon_L, \tag{5}$$

where E_V, E_D and E_T are the microplane elastic moduli which are always positive and, in the case of virgin loading, are constant and expressed in terms of Young's modulus E (macroscopic) and Poisson's ratio v;

$E_V = E/(1-2v)$, $E_D = 5E/[(1+v)(2+3\eta)]$ and $E_T = \eta E_D$. The value $\eta = 1$ is, for various reasons, optimal (Bažant and Prat, 1988; Carol and Bažant, 1997). For unloading and reloading, E_V, E_D and E_T are functions of the current strain and the maximum strain reached so far. The stress–strain boundaries, which may be regarded as strain dependent yield limits, consist of the following conditions:

$$\begin{aligned} &\sigma_N \leqslant F_N(\epsilon_N), \qquad F_V^-(\epsilon_V) \leqslant \sigma_V \leqslant F_V^+(\epsilon_V), \qquad F_D^-(\epsilon_D) \leqslant \sigma_D \leqslant F_D^+(\epsilon_D), \\ &|\sigma_M| \leqslant F_T(\sigma_N, \epsilon_V, \epsilon_I, \epsilon_{III}), \qquad |\sigma_L| \leqslant F_T(\sigma_N, \epsilon_V, \epsilon_I, \epsilon_{III}), \end{aligned} \tag{6}$$

Except for the last two conditions, which model friction, interactions among various components need not be considered, since the cross effects are adequately captured by interactions among various microplane due to the kinematic constraint. The unloading conditions are formulated separately for each microplane component. Unloading occurs when the incremental work of a microplane component becomes negative, i.e. when, separately for each component:

$$\sigma_N \Delta\epsilon_N \leqslant 0, \qquad \sigma_V \Delta\epsilon_V \leqslant 0, \qquad \sigma_D \Delta\epsilon_D \leqslant 0, \qquad \sigma_M \Delta\epsilon_M \leqslant 0, \qquad \sigma_L \Delta\epsilon_L \leqslant 0. \tag{7}$$

Reloading for any component occurs when the corresponding condition among the foregoing is violated while the corresponding condition (6) is a strict inequality. The expressions for the boundary functions, identified for model M4 by fitting the available test data, are given in Appendix A.

3. Basic concept of nonlocal model

The nonlocal model, in general, consists in replacing a certain local variable $f(\mathbf{x})$, characterizing the softening damage of material, by its nonlocal counterpart $\bar{f}(\mathbf{x})$. The nonlocal operator is defined as

$$\bar{f}(\mathbf{x}) = \int_V \hat{\alpha}(\mathbf{x}, \boldsymbol{\xi}) f(\boldsymbol{\xi}) \, \mathrm{d}V(\boldsymbol{\xi}), \tag{8}$$

where V is the volume of the structure, $\mathbf{x}$, $\boldsymbol{\xi}$ are the coordinates vectors, and $\hat{\alpha}(\mathbf{x}, \boldsymbol{\xi})$ is the normalized nonlocal weight function:

$$\hat{\alpha}(\mathbf{x}, \boldsymbol{\xi}) = \frac{\alpha(\mathbf{x} - \boldsymbol{\xi})}{\int_V \alpha(\mathbf{x} - \boldsymbol{\zeta}) \, \mathrm{d}V(\boldsymbol{\zeta})}. \tag{9}$$

Here $\alpha(\mathbf{x} - \boldsymbol{\xi})$ is the basic nonlocal weight function for an unbounded medium; $\int_V \alpha(\mathbf{x} - \boldsymbol{\zeta}) \, \mathrm{d}V(\boldsymbol{\zeta})$ is a constant if the unrestricted averaging domain does not tend to protrude outside the boundaries. The weight function $\alpha(\mathbf{x} - \boldsymbol{\xi})$ is often taken as a bell-shaped function. Its analytical expression, used in this work, is:

$$\alpha(\mathbf{x}, \boldsymbol{\xi}) = \begin{cases} (1 - |\mathbf{x} - \boldsymbol{\xi}|^2 / R^2)^2 & \text{if } 0 \leqslant |\mathbf{x} - \boldsymbol{\xi}| \leqslant R, \\ 0 & \text{if } R \leqslant |\mathbf{x} - \boldsymbol{\xi}|, \end{cases} \tag{10}$$

where R is a parameter proportional to the material characteristic length l (Fig. 2 for one- and bi-dimensional case), $R = \rho_0 l$. Note that $|\mathbf{x} - \boldsymbol{\xi}| = \sqrt{(x_i - \xi_i)^2}$ and $\alpha(\mathbf{x}, \mathbf{x}) = 1$. The coefficient ρ_0 is determined so that the volume under function α be equal to the volume of the uniform distribution ($\rho_0 = 15/16 = 0.9375$ for 1D, $\rho_0 = \sqrt[3]{3/4} = 0.9086$ for 2D, $\rho_0 = \sqrt[3]{35}/4 = 0.8178$ for 3D).

The averaging function (10) is doubtless a simplification. Properly, α should also depend on the orientation of the principal stress axes at $\boldsymbol{\xi}$ and $\mathbf{x}$, as proposed by Bažant (1994) on the basis of micromechanics analysis of a random system of interacting and growing microcracks. A combination of that kind of nonlocal continuum with the microplane model was implemented by Ožbolt and Bažant (1996), and allowed an improved representation of opening and shear fractures with the same material model (Bažant and Ožbolt, 1990). However, the implementation is more complicated and is not needed for the present purpose.

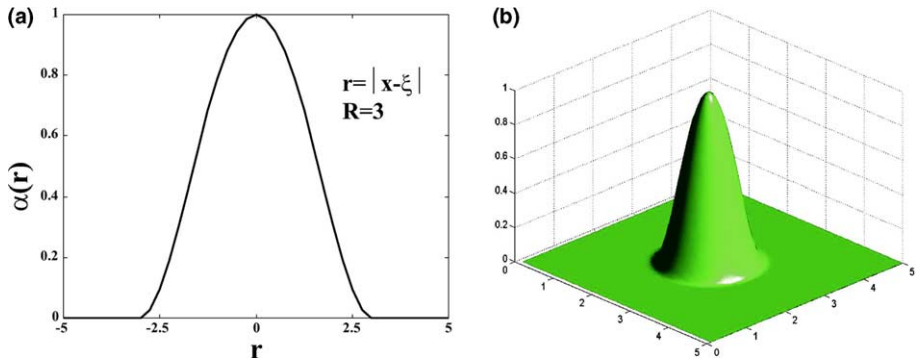

Fig. 2. Normalized nonlocal bell-shaped weight function: (a) in one-dimension, (b) in two-dimension.

Vermeer and Brinkgreve (1994), Strömberg and Ristinmaa (1996), and Planas et al. (1996) (see also Bažant and Planas, 1998), introduced a refinement of the standard nonlocal formulation, here called over-nonlocal, in which the averaged nonlocal variable $\bar{f}(\mathbf{x})$ is replaced by the following over-nonlocal variable:

$$\hat{f}(\mathbf{x}) = m\bar{f}(\mathbf{x}) + (1-m)f(\mathbf{x}) \tag{11}$$

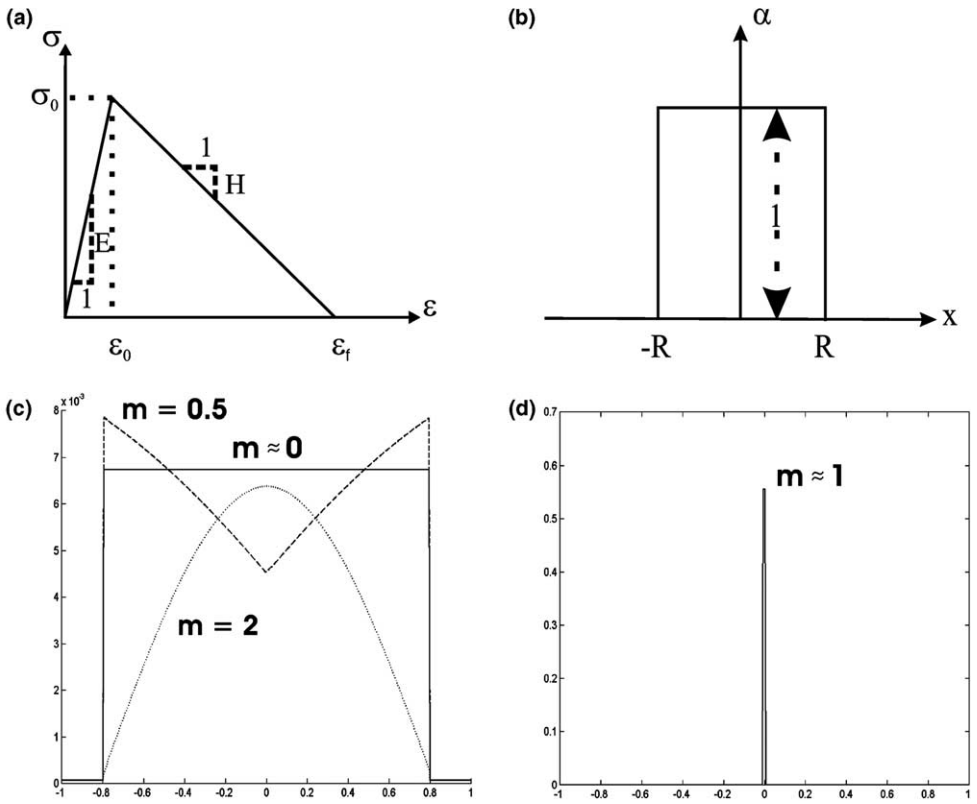

Fig. 3. (a) Linear softening; (b) rectangular weight function; (c) strain profiles in the localization band for various values of m; (d) strain profiles in the localization band for $m \approx 1$.

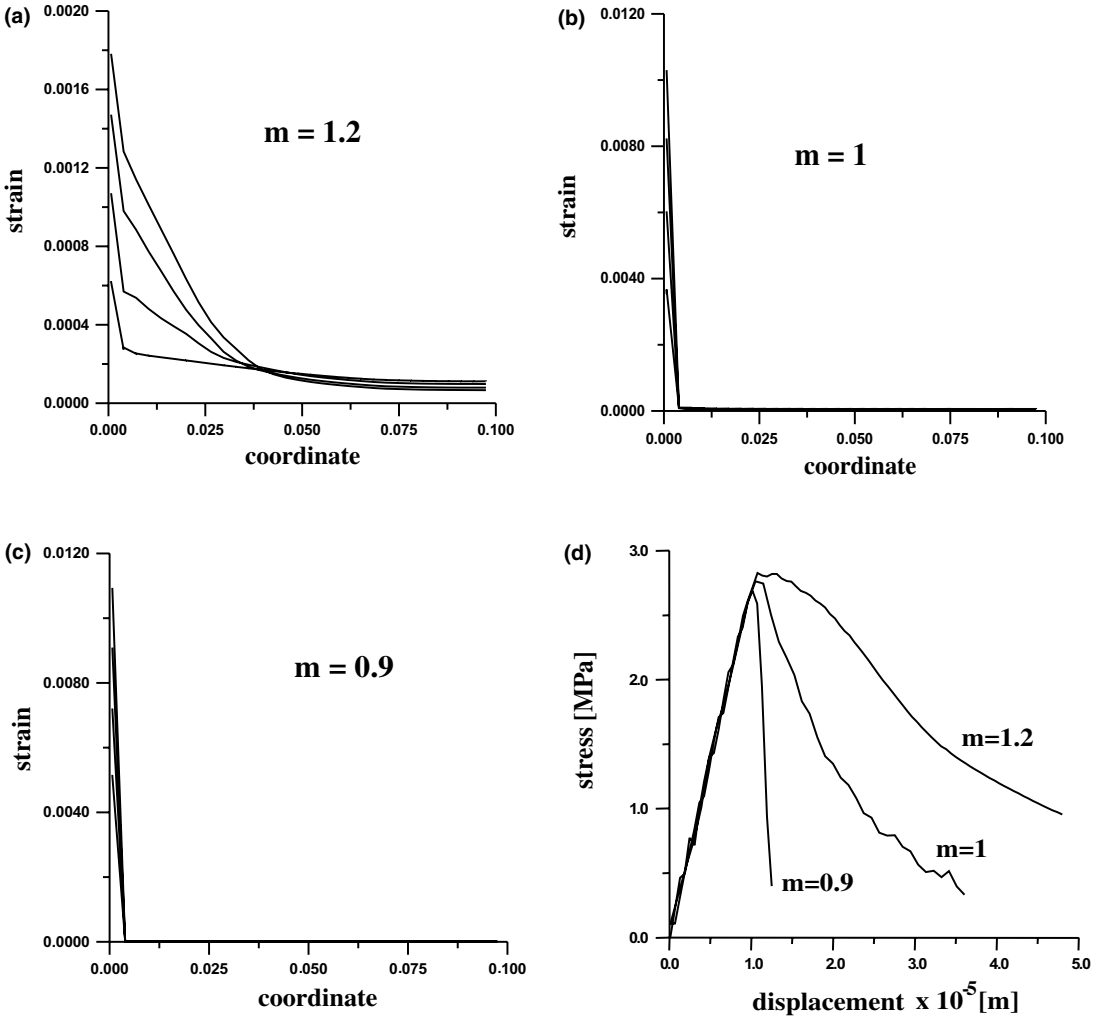

Fig. 4. Strain-softening bar: (a) strain profile along the bar for $m = 1.2$; (b) strain profile along the bar for $m = 1$; (c) strain profile along the bar for $m = 0.9$; (d) stress–displacement curves for different values of m.

in which $\mathbf{x}$ is the nonlocal variable obtained from Eq. (8), and m is an empirical coefficient. Strömberg and Ristinmaa (1996) called it the 'mixed local and nonlocal model'. Planas et al. (1996) called this formulation a 'nonlocal model of the second kind'. The results of both confirmed the spurious localization to be avoided even at large strains if $m > 1$. Planas et al. (1996) rigorously proved, for a uniaxial stress field, that the localization zone is finite if and only if $m > 1$. It was also proven (Bažant and Planas, 1998) that, for the special case of uniaxial stress, the formulation with $m > 1$ is equivalent, in terms of strain rate distribution at bifurcation from a uniform strain state, to the nonlocal damage model of Pijaudier-Cabot and Bažant (1987).

4. Nonlocal generalization of microplane model

The original nonlocal model of Bažant (1984) and Bažant et al. (1984) led to spurious zero-energy instability modes (Bažant and Cedolin, 1991), which had to be suppressed by an artificial elastic restrain, at

the cost of making softening to zero stress unattainable. These difficulties can be traced to the nonlocality of the incremental elastic strains. On the other hand, according to the later findings of Pijaudier-Cabot and Bažant (1987) and Bažant and Pijaudier-Cabot (1988), the nonlocality of inelastic strain is free of this undesirable side effect.

The microplane model differs from the classical tensorial model of plasticity and continuum damage by the fact that the stress–strain boundaries, which define the inelastic strain, depend on the total strain only. This suggests a nonlocal generalization in which the stress–strain boundaries are evaluated from the nonlocal total strains (instead of being evaluated from the local total strain, with the nonlocal averaging postponed until after the inelastic strains have been evaluated).

Based on these considerations, a proposal is here made for a new kind of nonlocal formulation in which the elastic stress increments are local and the boundaries in Eq. (6) are modified as follows:

$$\begin{aligned} &\sigma_N \leqslant F_N(\hat{\epsilon}_N), \qquad \sigma_V \leqslant F_V^+(\hat{\epsilon}_V), \qquad F_D^-(\hat{\epsilon}_D) \leqslant \sigma_D \leqslant F_D^+(\hat{\epsilon}_D), \\ &|\sigma_M| \leqslant F_T(\sigma_N, \hat{\epsilon}_V, \hat{\epsilon}_I, \hat{\epsilon}_{III}), \qquad |\sigma_L| \leqslant F_T(\sigma_N, \hat{\epsilon}_V, \hat{\epsilon}_I, \hat{\epsilon}_{III}). \end{aligned} \tag{12}$$

For the sake of generality, the arguments in these conditions are considered as over-nonlocal;

$$\hat{\epsilon}_V = \hat{\epsilon}_{kk}/3, \qquad \hat{\epsilon}_N = N_{ij}\hat{\epsilon}_{ij}, \qquad \hat{\epsilon}_D = \hat{\epsilon}_N - \hat{\epsilon}_V, \qquad \hat{\epsilon}_M = M_{ij}\hat{\epsilon}_{ij}, \qquad \hat{\epsilon}_L = L_{ij}\hat{\epsilon}_{ij}, \tag{13}$$

where $\hat{\epsilon}_{ij} = m\bar{\epsilon}_{ij} - (m-1)\epsilon_{ij}$, ϵ_{ij} are the Cartesian components of $\boldsymbol{\epsilon}$, and the over-bar denotes the nonlocal counterpart of the variable as defined in Eq. (8). The standard nonlocality is the special case for $m = 1$.

Considering a state of uniaxial tension, σ, in the direction normal to a localization band, we can easily explore the basic properties of the model. The proposed nonlocal formulation is analyzed for the case of a uniaxial stress–strain relation of the form:

$$\text{for} \quad x \in \mathscr{F} : \quad \sigma = f[\bar{\epsilon}(x)] \quad \text{else} : \quad \sigma = E\epsilon(x). \tag{14}$$

Stress σ is assumed to be uniform, $\mathscr{F}$ is the localization band of softening material, and f is a monotonically decreasing function approaching 0 for $\bar{\epsilon} \to \infty$. Let us check whether the displacement profile $\epsilon(x)$ could have the following expression:

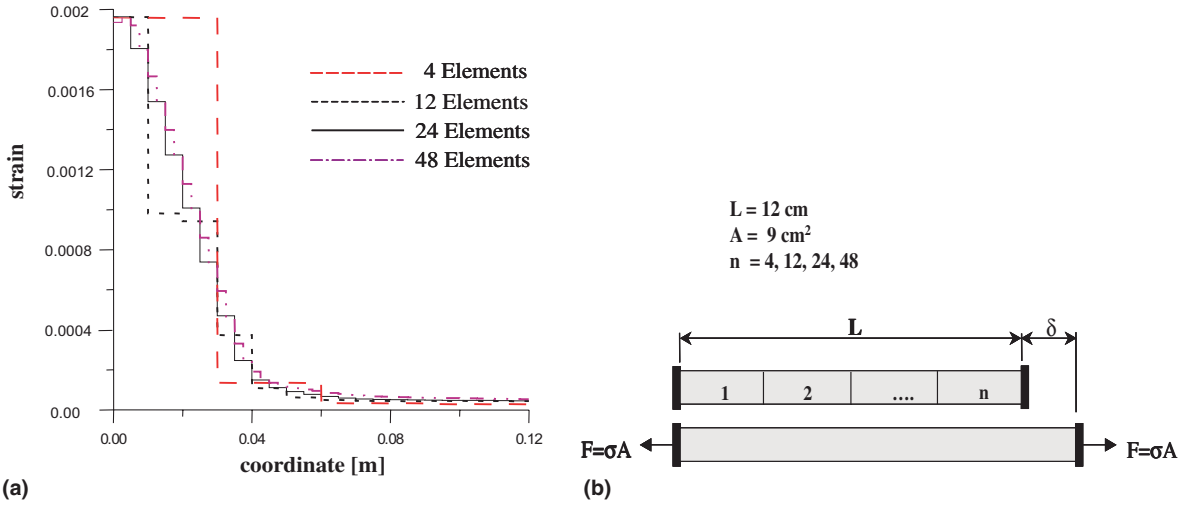

Fig. 5. (a) Longitudinal strain along the bar for various degrees of mesh refinement; (b) Geometry description for the one dimensional problem.

$$\epsilon(x) = \frac{\sigma}{E} + \epsilon_{\mathscr{F}}(x), \tag{15}$$

where $\epsilon_{\mathscr{F}}(x)$ is the unknown strain profile in the localization band $\mathscr{F}$. For the sake of simplicity, we assume, in $\mathscr{F}$, a linear softening function, and for the weight function α the rectangular function (Fig. 3b).

Considering the over-nonlocal refinement and the linear softening function (Fig. 3a), we can rewrite Eq. (14) as

$$\text{for} \quad x \in \mathscr{F} : \quad \sigma = \sigma_0 - H(m\bar{\epsilon}(x) + (1-m)\epsilon(x) - \epsilon_0). \tag{16}$$

Averaging the strain in Eq. (15), the nonlocal strain $\bar{\epsilon}(x)$ in Eq. (16) has, according to Eq. (8), the following expression:

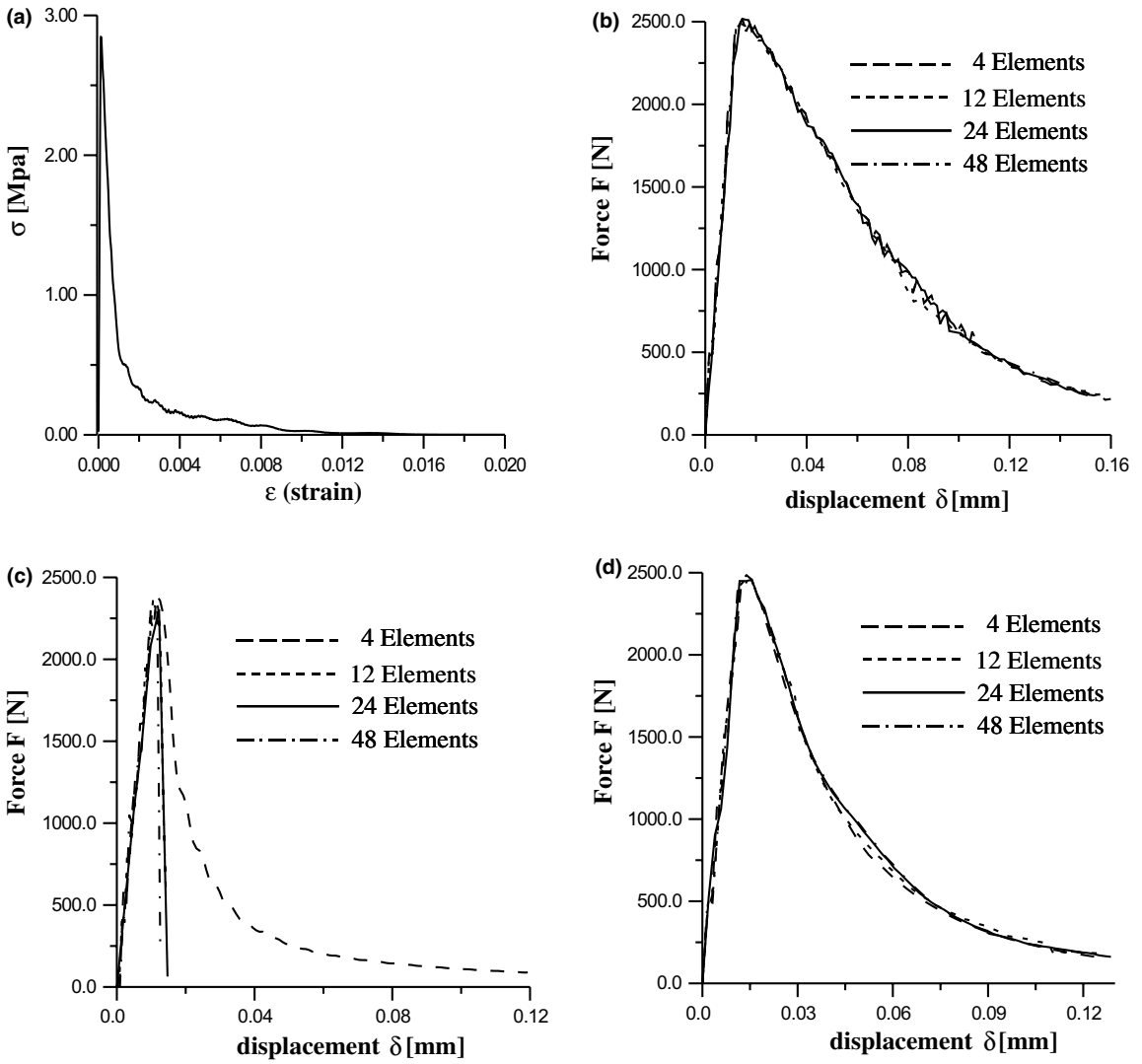

Fig. 6. Load–displacement curves for various degrees of mesh refinement: (a) local stress–strain law; (b) nonlocal microplane model; (c) local microplane model; (d) nonlocal microplane model obtained through the averaging of the inelastic strain (Appendix B).

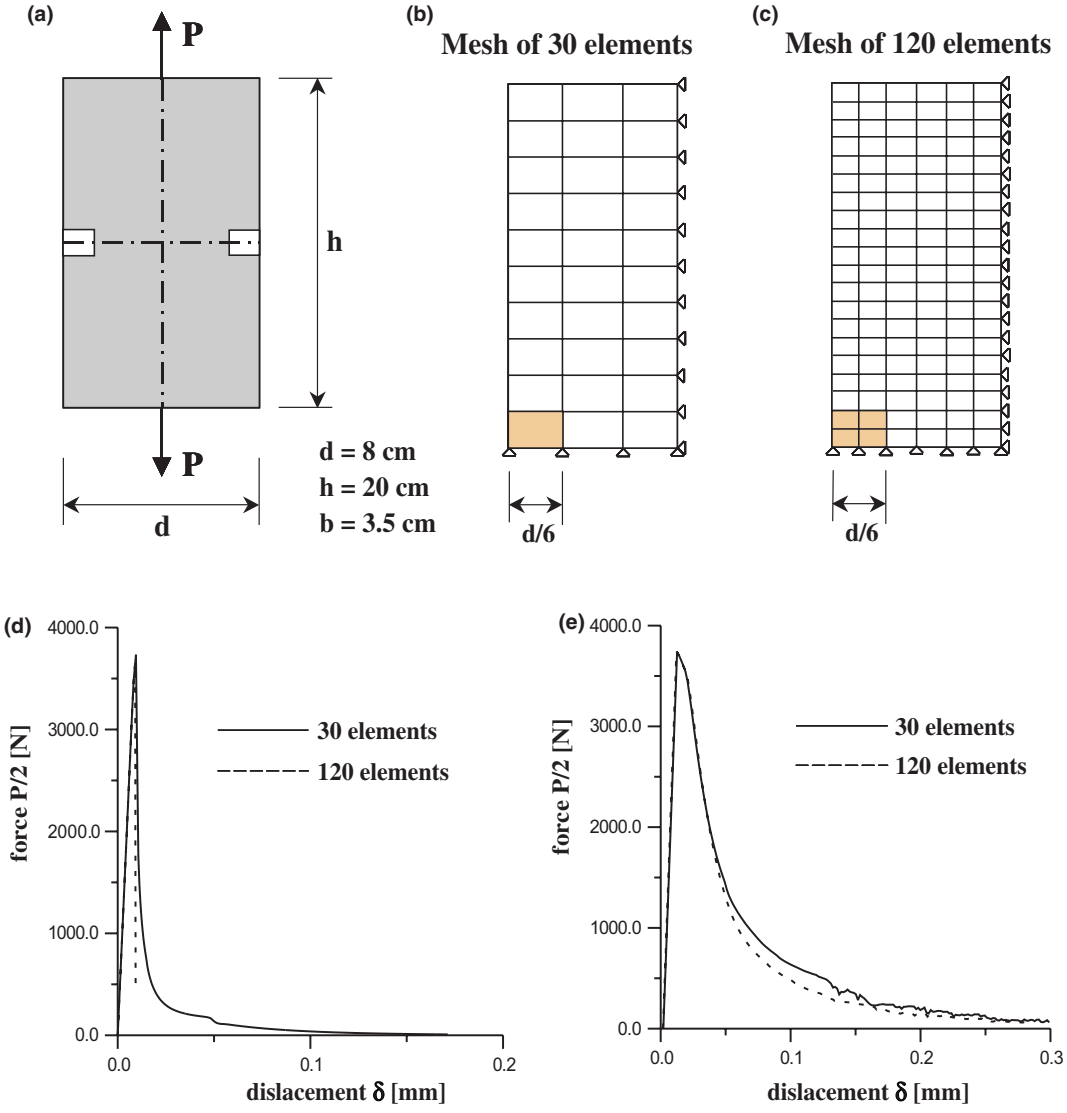

Fig. 7. (a) Geometry of the rectangular panel; (b) mesh with 30 finite elements; (c) mesh with 120 finite elements. Load–displacement curves for the two different refined meshes: (d) local microplane model (e) nonlocal microplane model.

$$\bar{\epsilon}(x) = \frac{1}{l}\left(l\frac{\sigma}{E} + \int_V \epsilon_{\mathscr{F}}(\xi)\alpha(\xi - x)\,\mathrm{d}\xi\right), \tag{17}$$

where, for a very long bar (extending from $-\infty$ to $+\infty$), $l = \int_{-\infty}^{+\infty} \alpha(\xi - x)\,\mathrm{d}\xi = \text{constant}$. Since Eq. (17) is defined in the localization band $\mathscr{F}$, and $\epsilon_{\mathscr{F}}(x) = 0$ for $x \notin \mathscr{F}$, we can evaluate the integral in Eq. (17) from $-h/2$ to $h/2$, where h is the length of localization zone. Substituting Eq. (17) into Eq. (16), we obtain:

$$B = \frac{m}{l}\int_{-h/2}^{h/2} \epsilon_{\mathscr{F}}(\xi)\alpha(\xi - x)\,\mathrm{d}\xi + (1 - m)\epsilon_{\mathscr{F}}(x), \tag{18}$$

where $B = \epsilon_0 - (\sigma - \sigma_0)/H - \sigma/E$ is a constant for a given uniaxial tension σ. Eq. (18) is a Fredholm integral equation of the second kind. For the sake of simplicity, Eq. (18) is solved numerically for a fixed value of h chosen as $h = 0.8l$. The bar is discretized into equal elements of constant $\epsilon_{\mathscr{F}}$. The integral is evaluated using a single integration point in the center of each element. The resulting linear system is solved for different values of m.

Fig. 3 shows the strain profiles, for different values of m. When the standard nonlocal model ($m \approx 1$) is considered, the strain distribution has the form of Dirac's δ-function (Fig. 3d). The total elongation of the bar can be considered as the sum of the elastic part, proportional to the bar length, and the inelastic part, independent of the bar length (as shown by Planas et al., 1993). Thus, this formulation ($m \approx 1$) is equivalent to a cohesive crack model. For $m < 1$, the strain distribution along the bar has an unrealistic shape: at the midlength of the localization zone, the value of the strain is less than its value at the boundaries, between the localization band and the rest of the bar, where there is no continuity of the strain profile (Fig. 3c). On the other hand, using $m > 1$, the strain profile is realistic: (1) it reaches the maximum value at the midlength of the localization band; (2) the strain is continuous at the boundaries, between the localization zone and the rest of the bar, where the inelastic strain continuously approaches the elastic one (Fig. 3c). A more rigorous and complete study, presented in Planas et al. (1996) and also in Bažant and Planas (1998, Chapter 13), which treats the length of the localization zone, h, as unknown in Eq. (18), shows that h is finite if and only if $m > 1$. It needs to be noted, however, that the present analysis with fixed h leads to an admissible solution for only one specific value of m, and so the profiles for other values of m do not represent actual

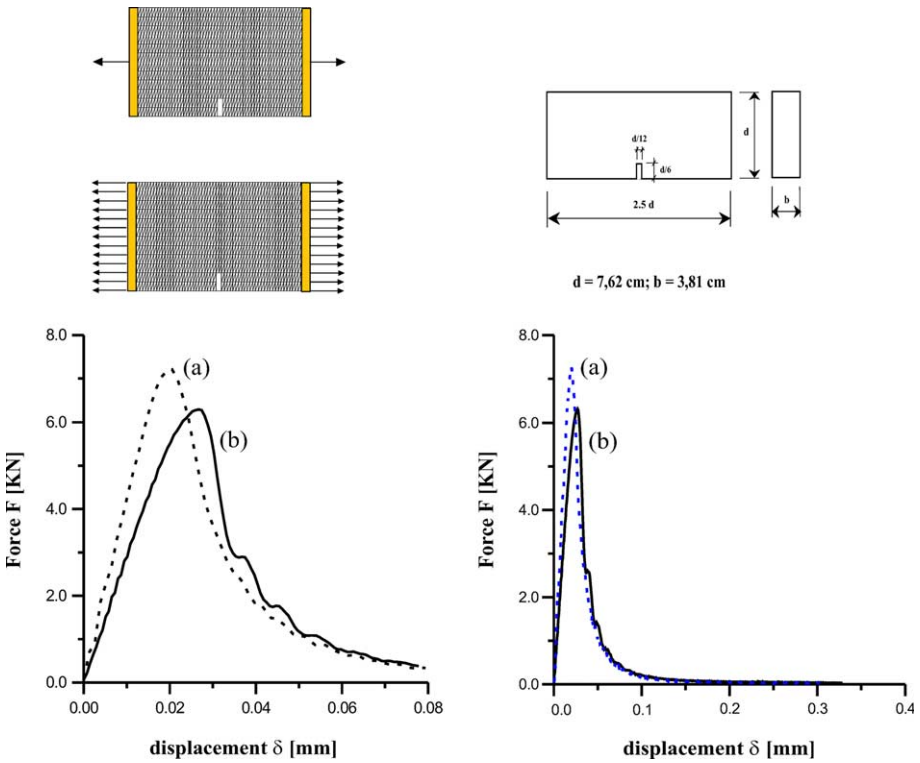

Fig. 8. Discretization meshes, geometry and load–deflection curves for the tensile test with uniform (a) and concentrated (b) displacement control.

admissible solutions. The actual solutions for other m would be characterized by other values of h and different profiles.

The behavior at very large strain, $\epsilon \to \infty$, across the localization band also be easily clarified. Noting that $\bar{\epsilon}(x) = \frac{1}{l}\int_V \epsilon(r+x)\alpha(r)\,\mathrm{d}r = \frac{1}{l}\left(\int_{\mathscr{F}} \epsilon(r+x)\alpha(r)\,\mathrm{d}r + \int_{\mathscr{E}} \frac{\sigma}{E}\alpha(r)\,\mathrm{d}r\right)$, where $V = \mathscr{F} \cup \mathscr{E}$, and taking into account Eq. (14), we must have, for $x \in \mathscr{F}$,

$$f\left(\frac{\sigma}{El}\int_{\mathscr{E}} \alpha(r)\,\mathrm{d}r + \frac{1}{l}\int_{\mathscr{F}} \alpha(r)\epsilon(x+r)\,\mathrm{d}r\right) = \sigma, \tag{19}$$

where $\lim f(\epsilon) = 0$ for $\epsilon \to \infty$. Now, if we assume that $\sigma \to 0$ and $\epsilon \to \infty$, this expression becomes $f(0+\infty) = 0 = \sigma$, and so this condition is satisfied. On the other hand, if we assume that $\sigma \to \sigma_r > 0$ at $\epsilon \to \infty$, the left-hand side in Eq. (19) is $f(\text{constant} + \infty) \to 0$, which cannot be equal to the right-hand side if the residual stress σ is finite. Hence, the residual stress across the band must vanish at very large displacement. This is not true for the classical nonlocal model with averaging of inelastic strain as shown numerically by Jirásek (1998).

The foregoing favorable properties of the nonlocal model are gained by making only the softening microplane stress–strain boundaries (strain-softening yield limits) function of the nonlocal strain. It is crucial to recognize that the elastic strains on the microplane (as well as any hardening inelastic strains) must depend only on the local strain, or else one would engender zero energy instability modes (such modes plagued the original nonlocal strain-softening continuum model, the so called imbricate model, and had to

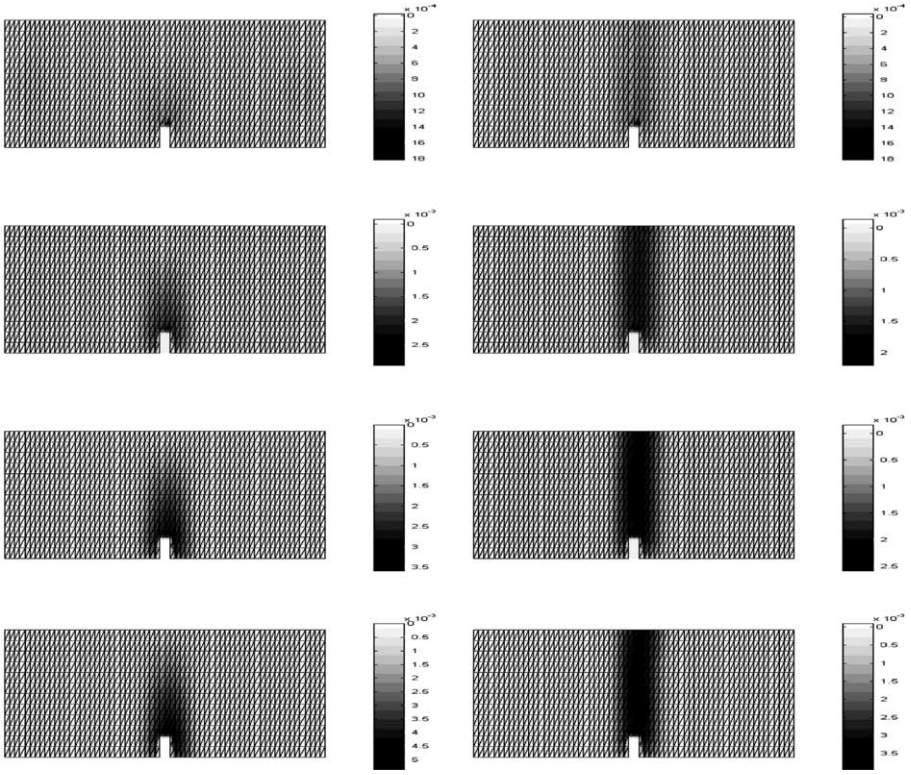

Fig. 9. Crack propagation for two different tensile tests. Left: for the concentred load. Right: for the distributed load.

be suppressed by parallel elastic coupling, which precluded the strain-softening from terminating with zero stress). This means that, in every constitutive law in which the softening depends on the strains, objectivity can be reached by making the softening function dependent on the nonlocal strains.

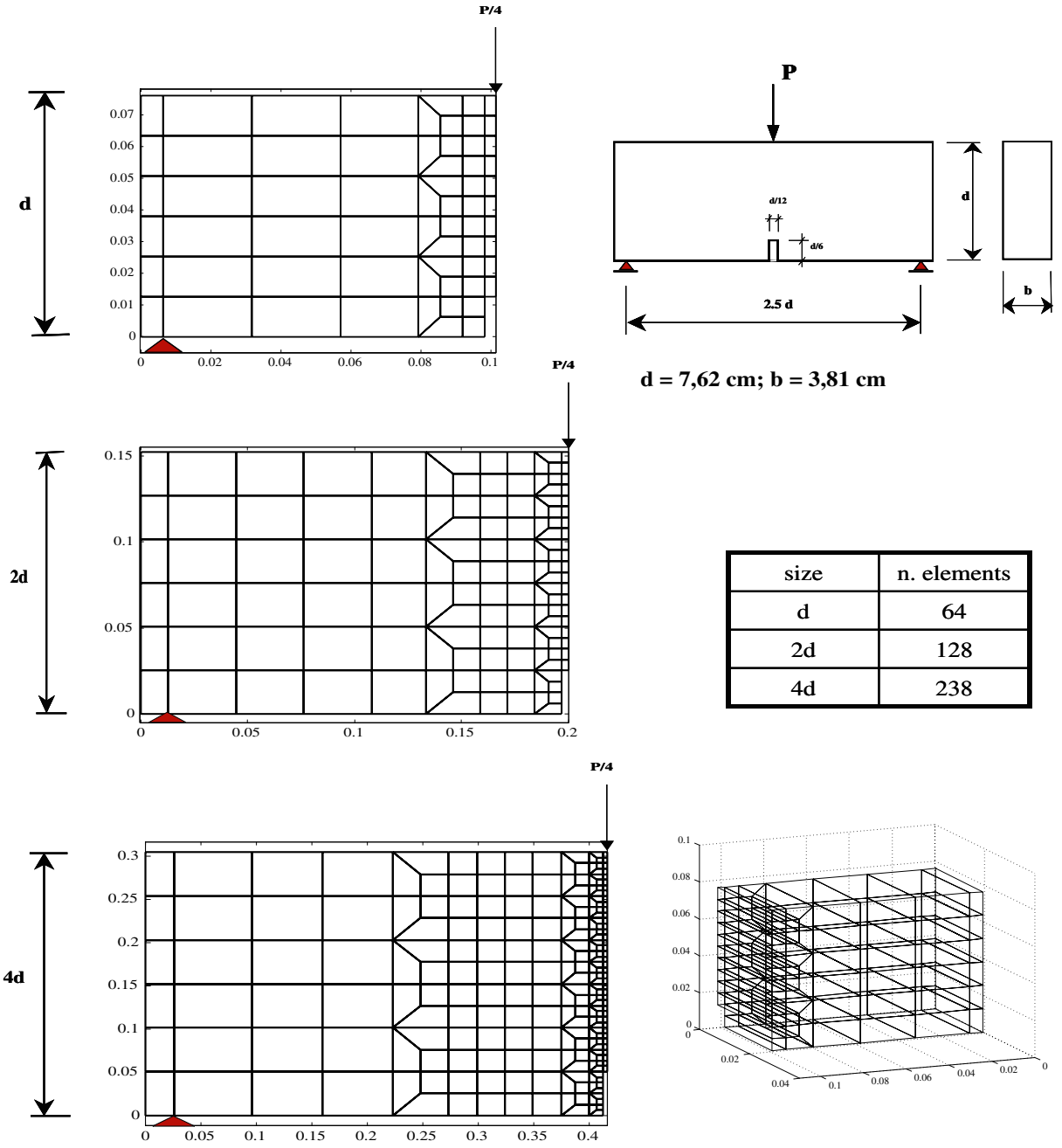

size	n. elements
d	64
2d	128
4d	238

Fig. 10. Three-point bending (test of Bažant and Pfeiffer, 1987): geometry description, and meshes used for three different beam sizes.

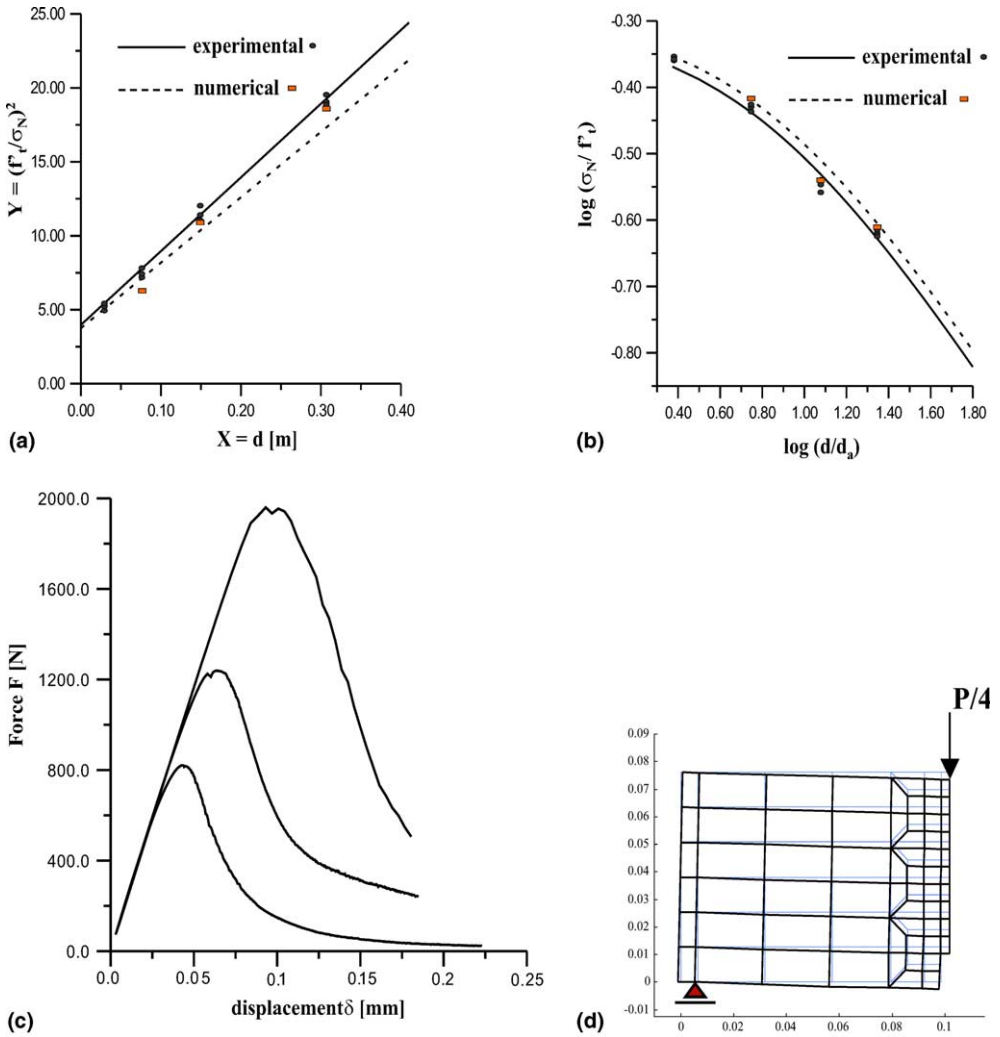

Fig. 11. Three-point bending (test of Bažant and Pfeiffer, 1987): comparison of test data and optimum fit of data by size effect law for three-point bending of Fig. 10: (a) linear regression plot; (b) Bažant's size effect law; (c) load–deflection curves for the three different sizes; (d) deformed specimen.

As an example, a one-dimensional strain-softening bar (with cross section area 4 cm^2 and length 10 cm) is numerically simulated for different values of m. The nonlocal generalization of microplane model M4 is used, with $l = 7.62$ cm. This numerical example confirms what was observed in the previous simplified model—only if the over-nonlocal formulation is used, a realistic description of the fracturing process is achieved. Fig. 4 shows that the fracturing strain is localized into a finite length, independently of the number of elements, only if m is larger than 1 (Fig. 4a). On the other hand, if the classical nonlocal model ($m = 1$) is adopted, the fracturing strain tends to localize into one element (Fig. 4b) even if the global response is correct (i.e., objective) in terms of the stress–displacement curve (Fig. 4d). Using a value of m less than 1 (i.e. $m = 0.9$), regularization is not achieved: the strain localizes into one element (Fig. 4c). Fig. 4d shows that, for $m = 0.9$, the stress–displacement curve shows a very steep post-peak branch approaching

a snap-back. The slope of the load–displacement diagram could be adjusted by changing the softening parameters, and so one cannot say that $m = 1$ gives a correct global response and $m = 0.9$ does not.

The reason why the classical continuum with the averaging of inelastic strains (or inelastic stresses) does not have the desired localization properties is that the inelastic strains (or inelastic stresses) in the models used are not functions of the nonlocal total strains. In this kind of models, no so much improvement was found. After adding a certain artificial feature, which makes m variable, satisfactory behavior can be achieved (see Appendix B).

5. Numerical studies

Without a nonlocal formulation (and without the use of the crack band model), the finite-element codes with strain softening exhibit unacceptable spurious mesh sensitivity. Especially, they cannot capture the size effect and crack propagation direction at a small angle with respect to the mesh line (directional bias of the mesh). To demonstrate that the present nonlocal formulation is free of these problems, seven examples of finite elements analysis using the over-nonlocal formulation with nonlocal stress–strain boundaries are presented. Monotonic loads and small strains and rotations are assumed. In examples number 1, 2 and 4, three-dimensional 8-node brick elements and implicit equilibrium solutions are used, while in the remaining examples a plane-strain analysis with explicit time integration is performed (the details of the numerical algorithm can be found in Appendix C).

1. *One dimensional bar.* Consider a straight bar of length L and a constant cross section of area A subjected to uniaxial tension (Fig. 5a). The material parameters are $l = 7.62$ cm, $m = 1.5$ and $E = 27{,}500$ MPa. The

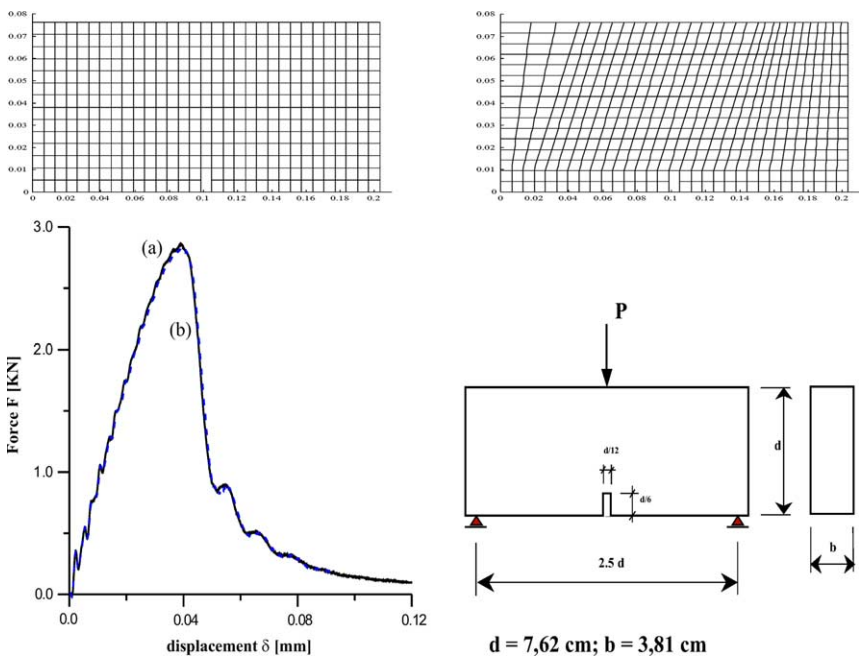

Fig. 12. Three-point bending example for testing the directional bias of mesh: geometry, meshes discretization, and load–displacement curve.

bar is loaded by a displacement applied at one end. To fix the place of damage, one quarter of the bar adjacent to the opposite end is assigned a Young's modulus 7.5% smaller than the rest. When the stress reaches the tensile strength limit, the softening starts in the weak element and, in a local formulation, all the other elements undergo elastical unloading. The nonlocal formulation of microplane model is able to prevent the localization of softening into one element. The strain distributions along the bar for various degrees of mesh refinement (4, 12, 24, 48 elements) are shown in Fig. 5b, and the load displacement curves are plotted in Fig. 6.

2. *Direct tensile test.* The rectangular panel in Fig. 7a, the same as considered by Bažant and Ožbolt (1990), is loaded in tension. The material parameters are $l = 7.62$ cm, $m = 1.5$ and $E = 27{,}500$ MPa. Because of symmetry, only one-quarter of the specimen is modeled. To fix the place of localization, a weak element,

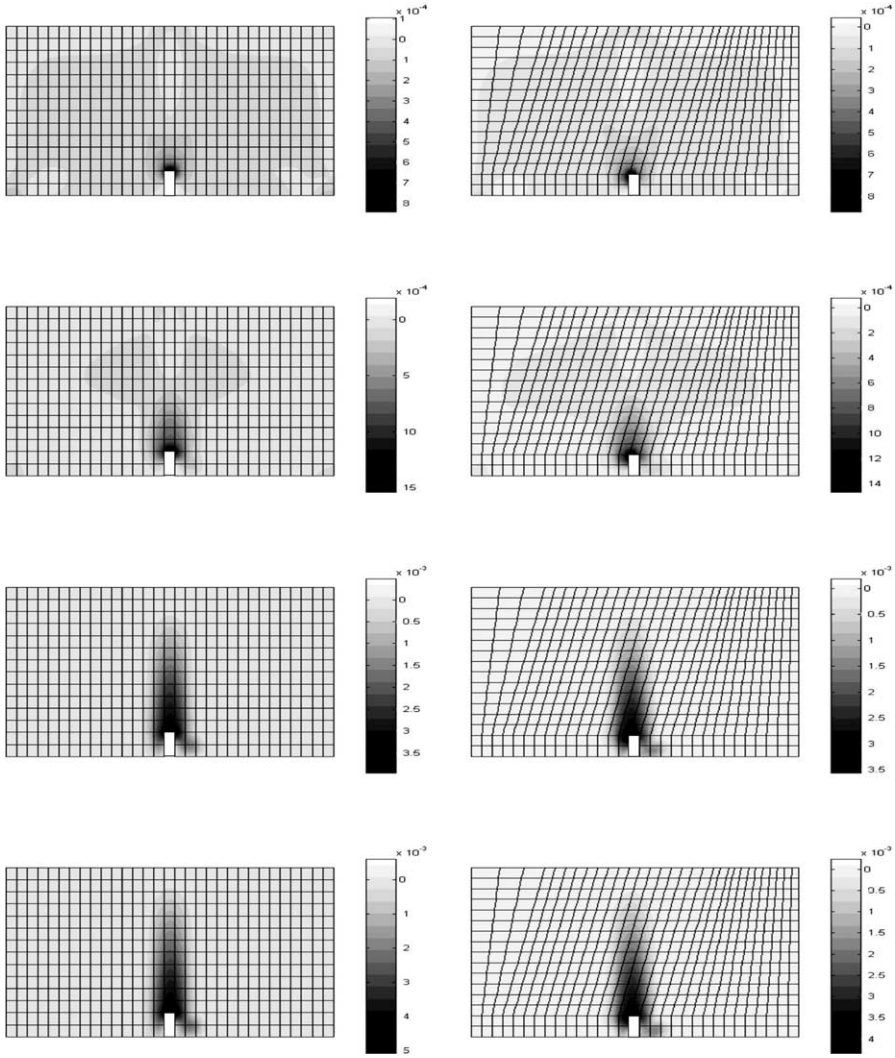

Fig. 13. Three-point bending example for testing the directional bias of mesh: crack distribution for the regular mesh (left) and for the slanted mesh (right) at different loading levels.

shown darker in Fig. 7, is introduced by reducing the elastic modulus by 7.5%. To show that the results are not mesh-sensitive, two finite element meshes are used: one with 30 (Fig. 7b) and the other one with 120 (Fig. 7c) finite elements. Fig. 7d and e shows the load–displacement curves for both meshes with local and nonlocal microplane model.

3. *Notched tensile test.* The test is described in Fig. 8. The Young's modulus of loading plates is 10-times higher than that of concrete. At the vertical edges, two types of displacement control are considered: a uniform displacement (non-rotating plates) and a point displacement (rotating plates), as shown in Fig. 8. The material parameters $l = 3.81$ cm, $m = 1.5$ and $E = 27{,}500$ MPa. Fig. 8 shows the load–displacement curves for both cases. The reader can clearly see, that the curves tend to zero when the displacements become large enough. In Fig. 9 one can see the crack distribution at different load levels, on the left side for rotating platens (realistic fracture propagation) and on the right side for non-rotating platens (the displacement being almost uniform across the ligament).
4. *Size effect in three-point bending.* One important consequence of nonlocality is the size effect. The three-point-bending tests of Bažant and Pfeiffer (1987) are considered. Fig. 10 shows the geometry, similar for each size, and the finite element meshes for three different specimen sizes, with size ratio 1:2:4. The smallest specimen depth is $d = 7.62$ cm. The thickness is $b = 3.81$ cm, for each size. The characteristic length is taken as $l = 3.175$ cm, and $m = 1.2$. The tensile strength of concrete and the elastic modulus are assumed as $f'_t = 2.8$ MPa and $E = 27{,}500$ MPa. The nominal stress at failure is defined as $\sigma_N = P_{\max}/\mathrm{d}b$, where $P_{\max}$ is the maximum load. Comparison with the test data is shown in Fig. 11. The curves in Fig. 11 represent a good fit of the present nonlocal model to the test results smoothed by Bažant's size effect law (Bažant, 1984; Bažant and Pfeiffer, 1987; RILEM Committee QFS, 2004):

$$\sigma_N = \frac{Bf'_t}{\sqrt{1 + D/D_0}}, \tag{20}$$

in which constants B and D_0 haven been determined from the test data (for the most general derivation from dimentional analysis and asymptotic matching, see Bažant, 2004). The average measured maximum loads for the three specimen sizes are 3105, 4635 and 7784 N, while those obtained from the present nonlocal model are 3260, 4876 and 8052 N, respectively, the errors being 4.9%, 5.2% and 3.4%.

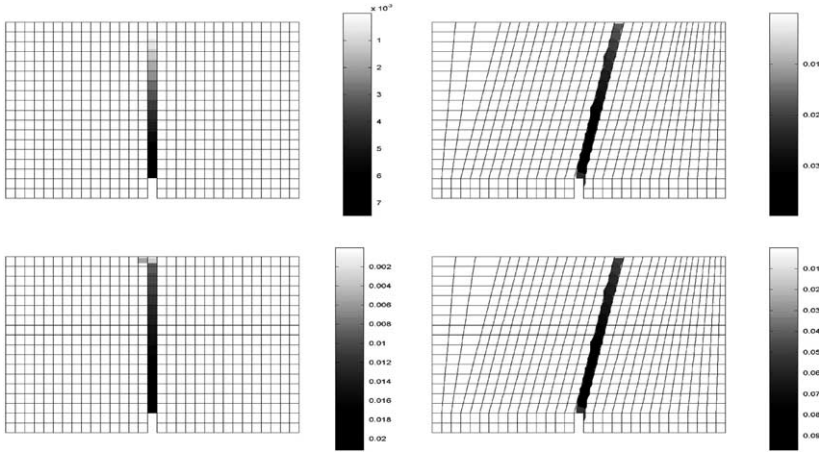

Fig. 14. Three-point bending example for testing the directional bias of mesh: crack distribution for the regular mesh (left) and for the slanted mesh (right) at different loading levels for the local microplane model M4.

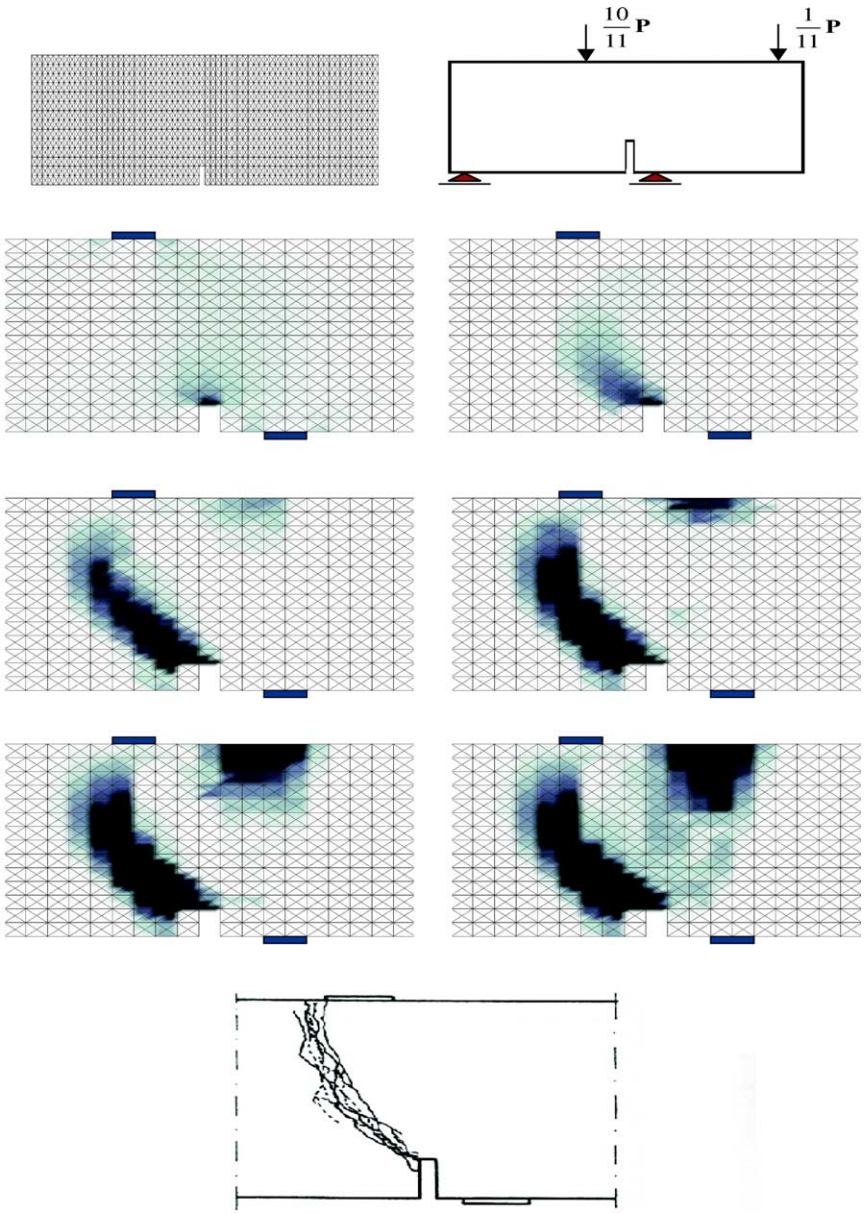

Fig. 15. Single-edge-notched beam subject to antisymmetric four-point shear loading: geometry, mesh discretization, and crack propagation for the four point shear (based on maximum principal strain).

5. *Elimination of directional mesh bias.* As mentioned before, the crack band model is not able to simulate a fracture propagation direction at small angle with the mesh line. This problem is studied using the specimen geometry, boundary condition and the meshes shown in Fig. 12. The lines of the slanted mesh are inclined by about 23°. Fig. 12 presents the load–displacement curves for both cases, for material parameters $l = 2.54$ cm and $E = 27{,}500$ MPa. One can see that both meshes give practically the same load–displacement curves, and the same is true for fracture propagation at different load levels (Fig. 13). Using a

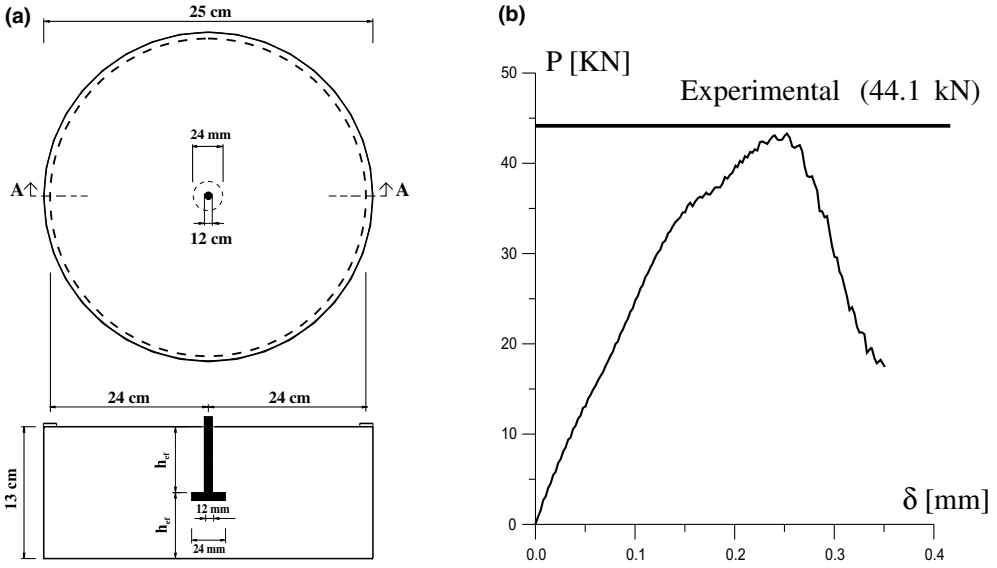

Fig. 16. Concrete cone pull-out of headed stud: (a) geometry description; (b) load–displacement curve compared with the maximum experimental load.

local microplane M4 with no regularization, the numerical solution exhibits a strong mesh bias for the fracture propagation (Fig. 14).

Antisymmetric four-point-shear. To show how the model is also able to predict a crack with a curved path, a notched specimen, subjected to an antisymmetric four-point shear loading, is considered (Fig. 15, a test used by Schlangen, 1993). The thickness of the beam is 38 mm. A mesh of 864 triangular 3-node elements is used (Fig. 15). The material parameters are $l = 1.905$ cm, $m = 1.25$ and $E = 27{,}500$ MPa. When the antisymmetric load is applied, a crack starts from the left corner of the notch and grows upwards to the left side of the loading platen. A second damage zone develops from the top surface of the specimen. Fig. 15 illustrates the crack propagation and cracking distribution at subsequent loading stages. Note that the experimentally observed curved crack path (Schlangen, 1993) is qualitatively reproduced, even if the second damage zone keeps growing for large displacement (this is due to the effect of the boundary conditions).

6. *Concrete cone pull-out of headed stud.* The case of headed anchor subjected to a tensile load is considered (UE Anchor Project, 2001). Many experimental data and some numerical studies have shown how the headed stud is able to transfer considerable tensile load without any reinforcement and demonstrated that the failure mechanism is a cone shaped fracture. Simulation of this problem by the cohesive crack model is difficult, not only because the crack path is not known a priori but also because a tensile fracture model is insufficient. The failure mode is not of a pure mode I type and a general triaxial constitutive law is necessary to reproduce correctly the entire response history. The proposed over-nonlocal microplane model is used to simulate the ultimate loads measured in pull-out test of a cast-in situ anchor, with bar diameter 12 mm, embedment length equal $h_{\mathrm{ef}} = 65$ mm, and head (stud) diameter 24 mm (see Fig. 16). The assessment of the parameters of the constitutive models is done by fitting the available mechanical properties of the concrete obtained from independent tests: compressive strength $f'_{\mathrm{c}} = 30.8$ MPa, tensile strength $f'_{\mathrm{t}} = 2.86$ MPa, Young modulus $E_{\mathrm{c}} = 35$ GPa, and fracture energy $G_{\mathrm{F}} = 64.5$ N/m, which gives $l = 3.6$ cm. Furthermore, $m = 1.25$. The steel bar is considered to be linearly elastic, with Young's modulus $E_{\mathrm{s}} = 210$ MPa and Poisson's ratio $v_{\mathrm{s}} = 0.3$. This assumption is justified by the fact that

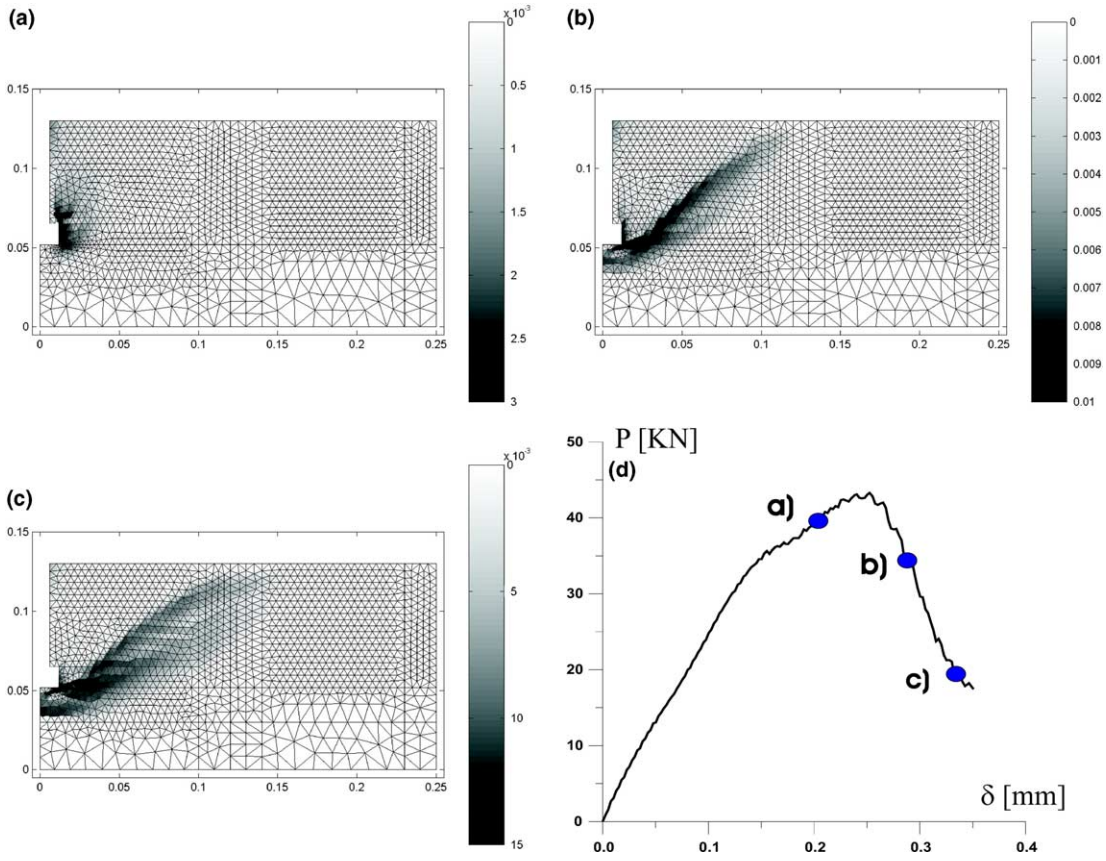

Fig. 17. Concrete cone pull-out of headed stud: evolution of the maximum principal strain for different values of the stud displacement.

the measured ultimate load $N_u = 44.1$ kN leads to a stress in the steel rod ($N_u/(0.25\pi\phi_s^2) = 389.9$ MPa) lower than the yielding strength. For numerical simulations by the microplane model, an axi-symmetric mesh of CST finite elements is used and the diameter of the concrete block is 25 cm. The mesh is constrained in the direction of the applied load, with sliding supports located at a distance of 23 cm from the axis of the stud. Fig. 16b compares the over-nonlocal simulation with the measured ultimate load. The numerical prediction (43.7 kN) is about 1.0% smaller than the experimental data (44.1 kN). Fig. 17 further shows the contours of the maximum principal strain computed by the microplane model at different values of the load-point displacement. As one can see, the strain localizes in a narrow localization band which starts from the bearing edge of the head and propagates towards the upper surface of the specimen, giving a fracture cone similar to observations in pull-out tests.

7. *Wave propagation in strain-softening bar.* Since spurious sensitivity to the mesh size appears not only for static but also for dynamic response, the problem of wave propagation along a one-dimensional bar has been investigated. In the one-dimensional wave equation for a strain-softening material, the characteristic lines and the wave speed become imaginary when strain-softening occurs. This means that the problem becomes elliptic, and the loss of hyperbolicity causes the initial value problem to become ill-posed. Thus, the physical problem cannot be realistically reproduced anymore. Let us consider the example of a one-dimensional bar (Bažant and Belytschko, 1985; Sluys, 1992) shown in

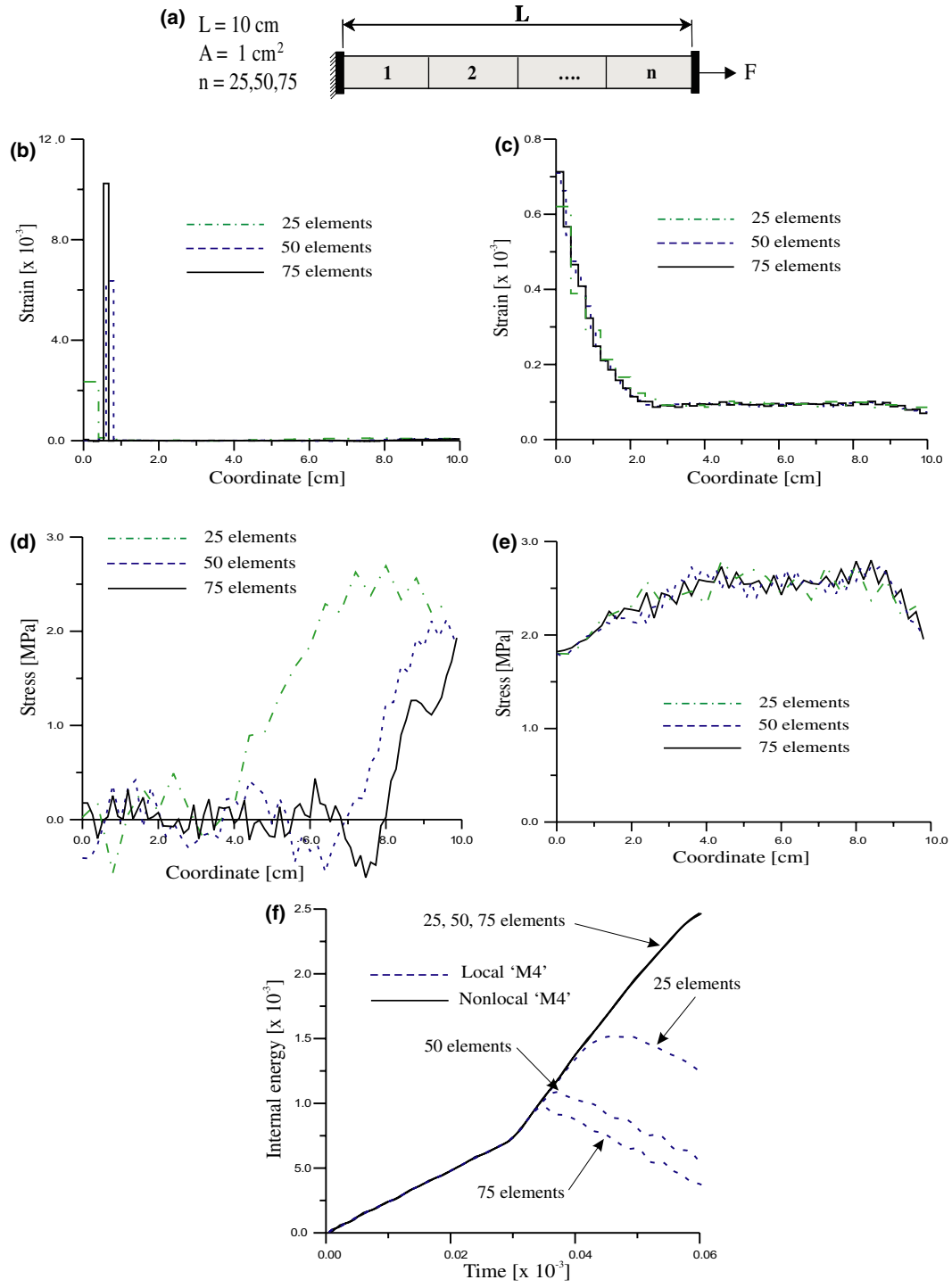

Fig. 18. Wave propagation in strain-softening bar: (a) geometry description; (b) strain localization for a local microplane model with different numbers of finite elements; (c) strain localization for a nonlocal microplane model with different finite element numbers; (d) stress wave reflection for a local microplane model with different number of finite elements; (e) stress wave reflection for a nonlocal microplane model with different finite elements number; (f) energy consumption in the bar.

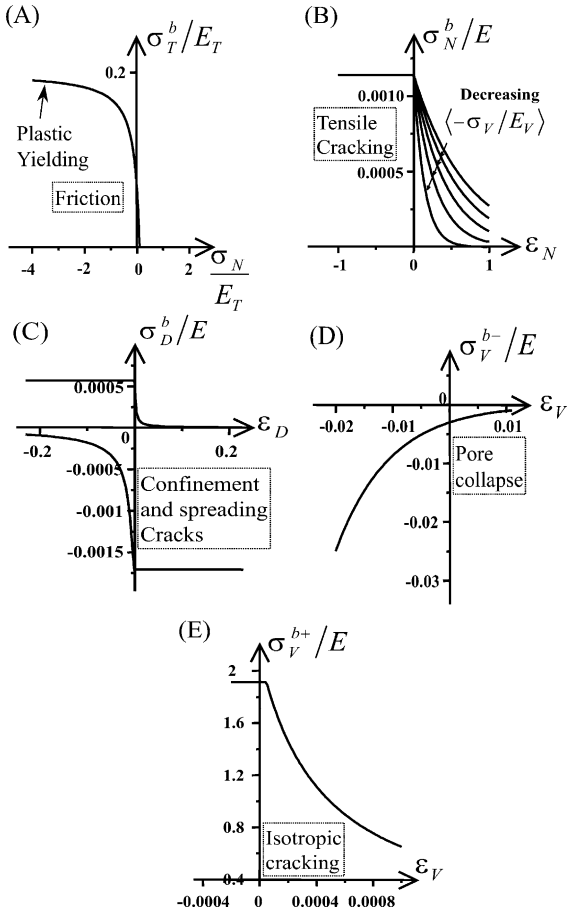

Fig. 19. Stress–strain boundaries for microplane model: (A) frictional boundary; (B) normal boundary; (C) deviatoric boundaries; (D) compression volumetric boundary; (E) tensile volumetric boundary (Bažant et al., 2000).

Fig. 18a, loaded by a tensile dynamic force at one end, while the other end is fixed. The bar is subdivided into 25, 50, and 75 elements. The material model is the nonlocal microplane model with the following material parameters: $l = 2.54$ cm, $m = 1.5$, $E = 27.500$ MPa, and $f'_c = 2.9$ MPa. The response of the bar is linearly elastic until the loading wave reaches the opposite boundary, where, due to the reflection of the wave, the stress is doubled and the crack starts to open. If a local strain-softening were used in the computation, the following problems (Bažant and Belytschko, 1985) would arise: (1) the strain would localize into an arbitrary finite element at the boundary where the reflection takes place (Fig. 18b); (2) the magnitude of the reflected wave would depend on the mesh refinement. The use of more elements would reduce the reflected stress wave (Fig. 18d); (3) the energy consumption would depend on the number of elements used; (4) decreasing the element size, the energy absorbed by the break of the bar would tend to vanish (Fig. 18f).

Using the nonlocal microplane model, mesh objectivity is achieved. The localization segment keeps a finite width, independent of the mesh discretization (Fig. 18c); the reflected wave is independent of the mesh refinement, as one can see from the stress profile after the reflection (Fig. 18e); and the energy dissipated by the break does not change with mesh refinement (Fig. 18f).

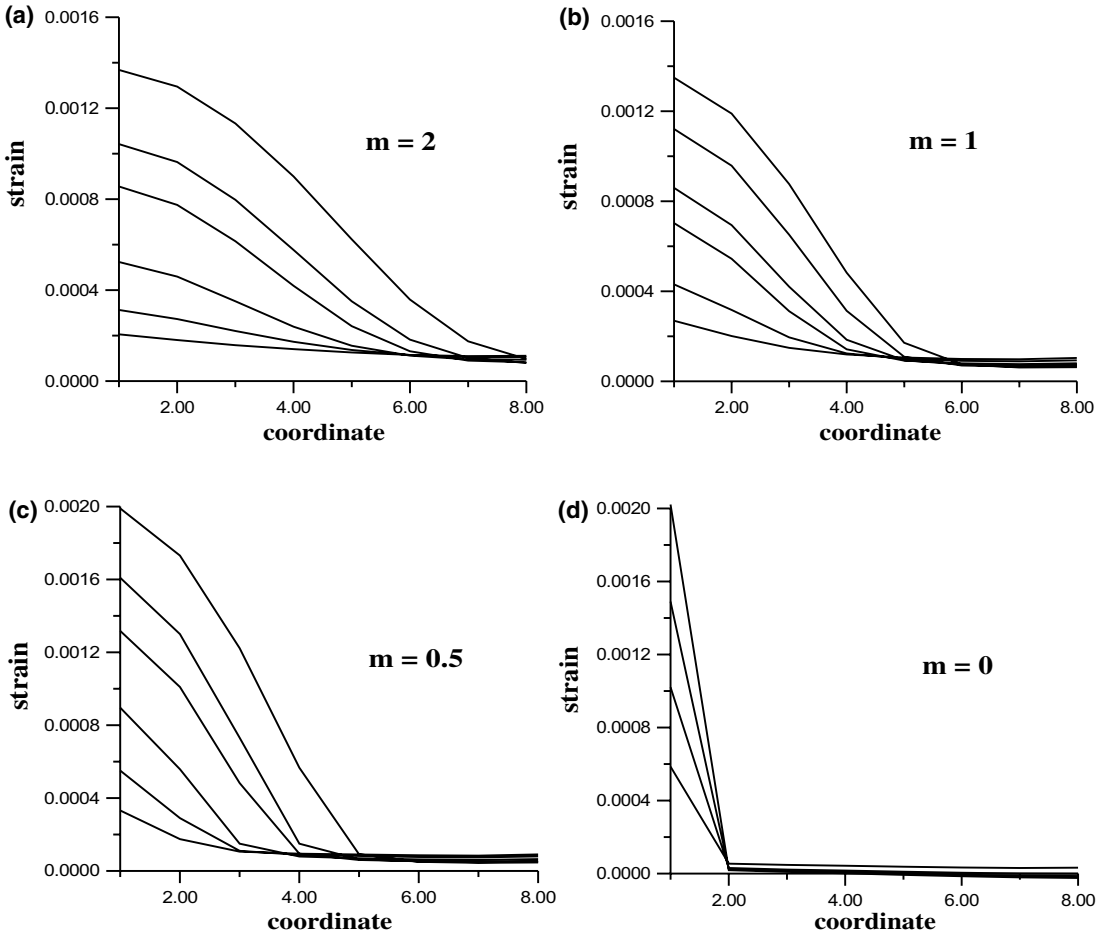

Fig. 20. Strain distribution along the bar for various values of m.

6. Conclusions

1. A particular characteristic of the microplane constitutive model M4 for cracking damage in concrete, is that the yield limits, called the stress–strain boundaries, exhibit softening as a function of the total strain. This feature, which is required in order to keep memory of the initial state, allows a simple and effective nonlocal generalization.
2. The proposed nonlocal generalization consists in replacing the total local strain by the total nonlocal strain, but only in the stress–strain boundaries. The elastic strains must still be expressed in terms of the local strains (or else spurious zero-energy modes of instability would arise).
3. By considering localization in a uniform tension field, it is demonstrated analytically as well as numerically that, with the proposed nonlocal model characterized by nonlocal softening boundaries: (1) the tensile stress across the band at very large strain does soften to zero, and (2) the cracking band retains a finite width even at very large tensile strains across the band only if one adopts the idea of Vermeer and Brinkgreve (1994). This idea consists in introducing an over-nonlocal variable, which is obtained as m times the nonlocal variable minus $(m-1)$ times the local variable (with $m > 1$).

4. The previously proposed nonlocal generalization, based on nonlocality of the inelastic part of strain, works well only in the early post-peak response. At very large strains across the band, the width of the cracking band does not retain a finite value, and the tensile stress across the band does not reduce to zero (which is called the stress locking). However, even if an over-nonlocal formulation is introduced, it works acceptably only if m is not a constant but a function of the tensile strain across the band (see Appendix B).
5. Numerical examples confirm the avoidance of spurious mesh sensitivity and orientational mesh bias, and demonstrate retention of a finite width of crack band as well as realistic modelling of the size effect—the main consequence of nonlocality.

Acknowledgements

The work of the first author and the visiting appointment of the second author at Northwestern University were partly supported under NSP grant CMS-9713944 to Northwestern University. The second author thank professor Luigi Cedolin for his guidance and the profitable discussions.

Appendix A. Microplane model M4

The constitutive microplane model M4, formulated and tested in Bažant et al. (2000) and Caner and Bažant (2000), is completely defined on the microplane level. All the material parameters except the Young's elastic modulus E are dimensionless. They are divided into the fixed (or constant) parameters, which are denoted as $c_1, c_2, \ldots, c_{26}$ and may be taken the same for all concretes, and the free parameters, which are denoted as k_1, k_2, k_3, k_4, and reflect the differences among different concretes. As introduced in the previous version, model M3, all the inelastic behavior is characterized on the microplane level by the so-called stress–strain boundaries, which may be regarded as strain-dependent yield limits and exhibit strain softening (Bažant et al., 1996a). Within the boundaries, the response is incrementally elastic, although the elastic moduli may undergo progressive degradation as a result of damage. Exceeding the boundary stress is never allowed. Travel along the boundary is permitted only if the strain increment is of the same sign as the total stress. Otherwise elastic unloading occurs. These simple rules for the boundaries suffice to obtain on the macrolevel the Bauschinger effect as well as realistic hysteresis loops during cyclic loading. Different microplanes enter the unloading or reloading regime at different times, which causes that the macroscopic response is quite smooth. Experience with data fitting has shown that each microplane stress component (normal, volumetric and deviatoric) boundaries can be assumed to depend only on its conjugate strain, i.e., the boundary stress σ_N depends only on ϵ_N, σ_V only on ϵ_V, and σ_D only on ϵ_D; see Fig. 19. Only in the shear boundary, which describes frictional interaction between two different stress components, the normal stress and the shear stress interact (Fig. 19A). The latest refinement, microplane model M5 (Bažant and Caner, 2002), which can also simulate transition to discrete fracture, is not used here (for further discussions, especially of the vertex affect, see Brocca and Bažant, 2000, and Caner et al., 2002).

Normal stress boundaries (tensile cracking, fragment pullout, crack closing). The tensile normal boundary is given as

$$\sigma_N^{\mathrm{b}} = F_N(\epsilon_N) = Ek_1c_1 \exp\left(-\frac{\langle \epsilon_N - c_1c_2k_1 \rangle}{k_1c_3 + \langle -c_4(\sigma_v/E_v) \rangle} \right), \tag{A.1}$$

where superscript b refers to the stress at the boundary; parameter c_3 controls mainly the steepness of the post-peak slope in uniaxial tension. The Macaulay brackets, defined as $\langle x \rangle = \max(x; 0)$, are used here and in several subsequent formulas to define horizontal segments of the boundaries, representing yield limits. The normal boundary is shown in Fig. 19B. Physically, its initial descending part characterizes the tensile

cracking parallel to the microplane, while its tail characterizes the frictional pullout of fragments and aggregate pieces bridging the crack from one of its faces. In addition, the closing of cracks after tensile unloading needs to be represented by a crack closing boundary, defined simply as $\sigma_N^{\mathrm{b}} = 0$ for $\epsilon_N > 0$; it prevents entry of the quadrant of positive ϵ_N and negative σ_N on the microplane level (however, in terms of uniaxial stress on the macrolevel, this quadrant can be entered because of microplane interactions and deviatoric stresses).

Deviatoric boundaries (spreading, splitting). The compressive deviatoric boundary controls the axial crushing strain of concrete in compression when the lateral confinement is too weak to prevent crushing. The tensile deviatoric boundary simulates the transverse crack opening of axial distributed cracks in compression and controls the volumetric expansion and lateral strains in unconfined compression tests. Both boundaries have similar shapes and similar mathematical forms:

$$\sigma_D^{\mathrm{b}} = F_D^{+}(\epsilon_D) = \frac{Ek_1c_5}{1 + \left(\frac{\langle \epsilon_D - c_5k_1c_6\rangle}{c_7k_1c_{20}}\right)^2} \quad \text{for } \sigma_D > 0, \tag{A.2}$$

$$\sigma_D^{\mathrm{b}} = F_D^{-}(-\epsilon_D) = \frac{Ek_1c_8}{1 + \left(\frac{\langle -\epsilon_D - c_8k_1c_9\rangle}{c_7k_1}\right)^2} \quad \text{for } \sigma_D < 0. \tag{A.3}$$

The deviatoric boundaries are shown in Fig. 19C. Because $\epsilon_D = 2/3(\epsilon_N - \epsilon_S)$, the deviatoric boundaries physically characterize the splitting cracks normal to the microplane, caused by lateral spreading, and their suppression by lateral confinement.

Frictional yield surface. The shear boundary physically represents friction. To reduce the computational burden, the frictional boundary can be applied not to the resultant shear stress σ_T but to the components σ_L and σ_M separately. The frictional boundary is nonlinear. It is a hyperbola starting with a finite slope at a certain finite distance from the origin on the tensile normal stress axis. This distance is gradually reduced to zero with increasing damage quantified by the volumetric strain. Thus, when the volumetric strain is small, the boundary provides a finite cohesive stress, which then decreases to zero with increasing volumetric strain. As the compressive stress magnitude increases, it approaches a horizontal asymptote. The friction boundary is expressed as

$$\sigma_T^{\mathrm{b}} = F_T(-\sigma_N) = \frac{E_Tk_1k_2c_{10}\langle -\sigma_N + \sigma_N^0\rangle}{E_Tk_1k_2 + c_{10}\langle -\sigma_N + \sigma_N^0\rangle}\psi(\epsilon_I, \epsilon_{III}), \tag{A.4}$$

where

$$\sigma_N^0 = E_Tk_1c_{11}\exp\left(-\frac{\langle \epsilon_V - c_{24}k_1\rangle}{c_{12}k_1}\right), \tag{A.5}$$

$$\psi(\epsilon_I, \epsilon_{III}) = \exp\left(-\frac{\langle \epsilon_I - c_{25}k_1\rangle}{c_{21}k_1}\cdot\frac{\langle -\epsilon_{III} + c_{26}k_1\rangle/(c_{22}k_1)]^{c_{23}}}{1 + [\langle -\epsilon_{III} + c_{26}k_1\rangle/(c_{22}k_1)]^{c_{23}}}\right). \tag{A.6}$$

Note that $\lim \sigma_{N\to\infty}\sigma_T = E_Tk_1k_2$, which represents a horizontal asymptote. The foregoing expression involves a finite cohesion, which can be calculated by setting $\sigma_N = 0$ and $\sigma_N^0 = E_Tk_1c_{11}$. When $\epsilon_V \gg 0$, the friction boundary actually passes through the origin; hence the cohesion becomes zero. The coefficient ψ, in Eqs. (A.6) and (A.4) was absent from the original model M4 (Bažant et al., 2000) and has been introduced by di Luzio (2002) in order to achieve a more realistic response when transverse compressive stresses are applied during tensile softening.

Volumetric boundaries (pore collapse, expansive breakup). The inelastic behavior under hydrostatic pressure (as well as uniaxial compressive strain) exhibits no strain-softening but progressively stronger

hardening caused primarily by collapse and closure of pores. It is simulated, by a compressive volumetric boundary in the form of a rising exponential (Fig. 19D). A tensile volumetric boundary needs to be imposed, too. These boundaries are:

$$\sigma_V^{\mathrm{b}} = F_V^-(-\epsilon_V) = -Ek_1k_3 \exp\left(-\frac{\epsilon_V}{k_1k_4}\right) \quad \text{for } \sigma_D < 0, \tag{A.7}$$

$$\sigma_V^{\mathrm{b}} = F_V^+(-\epsilon_V) = \frac{E_V k_1 c_{13}}{\left[1 + (c_{14}/k_1)\langle \epsilon_V - k_1 c_{13}\rangle\right]^2} \quad \text{for } \sigma_D > 0. \tag{A.8}$$

A.1. Unloading and stiffness degradation

To model unloading, reloading and cyclic loading with hysteresis, it is necessary to take into account the effect of material damage on the incremental elastic stiffness. For virgin loading as well as reloading of any component, the incremental (tangential) moduli are constant and equal to the initial elastic moduli E_V, E_D and E_T. An exception is the compressive hydrostatic reloading, for which, as experiments show, the response never returns to the virgin loading curve given by the compressive hydrostatic boundary. Rather, the slope E_V of reloading keeps being parallel to the boundary slope for the same ϵ_V, and thus the reloading response moves parallel to the boundary curve.

Unloading is assumed to occur when the work rate $\sigma\dot{\epsilon}$ (or increment $\sigma\Delta\epsilon$) becomes negative. This unloading criterion is considered separately for each microplane stress component. The following empirical rules for the incremental unloading moduli on the microplanes have been developed, with good results: for $\epsilon_V \leqslant 0$ and $\sigma_V \leqslant 0$:

$$E_V^U(-\epsilon_V, -\sigma_V) = E_V\left(\frac{c_{16}}{c_{16} - \epsilon_V} + \frac{\sigma_V}{c_{16}c_{17}E_V}\epsilon_V\right), \tag{A.9}$$

and for $\epsilon_V > 0$ and $\sigma_V > 0$:

$$E_V^U(\epsilon_V, \sigma_V) = \min[\sigma_V(\epsilon_V)/\epsilon_V, E_V], \quad E_D^U = (1 - c_{19})E_D + c_{19}E_D^S, \tag{A.10}$$

where, if $\sigma_D\epsilon_D \leqslant 0$: $E_D^S = E_D$; else

$$E_D^S = \min(\sigma_D/\epsilon_D, E_D), \quad E_T^U = (1 - c_{19})E_T + c_{19}E_T^S, \tag{A.11}$$

where, if $\sigma_T\epsilon_T \leqslant 0$: $E_T^S = E_T$; else $E_T^S = \min(\sigma_T/\epsilon_T, E_T)$. c_{15}, c_{16}, c_{17} are fixed dimensionless parameters, and superscript S denotes the secant modulus; c_{17} controls the unloading modulus, which equals the virgin elastic modulus for $c_{17} = 0$ and the secant modulus for $c_{17} = 1$.

Material parameters. The default values of the adjustable parameters, denoted as k_i, and the fixed parameters, denoted as c_i, and, are assumed as

$k_1 = 9.50 \times 10^{-5}$; $k_2 = 200.0$; $k_3 = 15.0$; $k_4 = 100.0$;
$c_1 = 1.25$; $c_2 = 0.22$; $c_3 = 2.0$; $c_4 = 70.0$; $c_5 = 2.70$; $c_6 = 1.30$;
$c_7 = 45.0$; $c_8 = 5.8$; $c_9 = 1.30$; $c_{10} = 0.73$; $c_{11} = 1.3$; $c_{12} = 12.5$;
$c_{13} = 0.27$; $c_{14} = 4500$; $c_{15} = 1.0$; $c_{16} = 0.02$; $c_{17} = 0.01$; $c_{18} = 1.0$;
$c_{19} = 0.4$; $c_{20} = 1.5$; $c_{21} = 5.0$; $c_{22} = 1.0$; $c_{23} = 4$; $c_{24} = 0.7$; $c_{25} = 1.55$;
$c_{26} = 10.0$.

These parameter values, along with $E = 27{,}500$ MPa, produce the uniaxial local stress–strain curve plotted in Fig. 6a. The scaling of the local constitutive law M4, needed to match the stiffness and strength of

different types of concrete, can be easily controlled through the adjustable parameters (Caner and Bažant, 2000).

Appendix B. Alternative approach with averaging of inelastic strains (or inelastic stresses)

An alternative nonlocal generalization, proposed in Bažant et al. (1996a,b), has also been examined. To prevent zero-energy modes of instability, the nonlocal concept must not be applied to the total strain ϵ. Rather, it must be applied to the inelastic strain (Pijaudier-Cabot and Bažant, 1987) or to some of its parameters. The general local constitutive law may be written as

$$\boldsymbol{\sigma} = \mathbf{E} : (\boldsymbol{\epsilon} - \boldsymbol{\epsilon}''), \tag{B.1}$$

where $\boldsymbol{\epsilon}''$ is the inelastic strain (fracturing strain, softening plastic strain, etc.) and all the variables are evaluated at $\mathbf{x}$. A nonlocal version of (B.1) can simply be obtained by replacing the local inelastic strain $\boldsymbol{\epsilon}''$ by nonlocal $\bar{\boldsymbol{\epsilon}}''$:

$$\boldsymbol{\sigma} = \mathbf{E} : (\boldsymbol{\epsilon} - \bar{\boldsymbol{\epsilon}}''), \qquad \bar{\boldsymbol{\epsilon}}''(\mathbf{x}) = \int_V \hat{\alpha}(\mathbf{x}, \boldsymbol{\xi}) \boldsymbol{\epsilon}''(\boldsymbol{\xi}) \, \mathrm{d}V(\boldsymbol{\xi}), \tag{B.2}$$

where $\hat{\alpha}(\mathbf{x}, \boldsymbol{\xi})$ is given by Eq. (9).

The constitutive model is here considered to be in an explicit form which gives the stress $\boldsymbol{\sigma}$ as a function of the total strain $\boldsymbol{\epsilon}$, i.e. $\boldsymbol{\sigma} = \boldsymbol{\sigma}(\boldsymbol{\epsilon})$, which is the case of microplane model M4 (as well as the preceding model M3; Bažant et al., 1996a,b). Then the local inelastic strain may be calculated as

$$\boldsymbol{\epsilon}'' = \boldsymbol{\epsilon} - \mathbf{C} : \boldsymbol{\sigma}(\boldsymbol{\epsilon}), \qquad \mathbf{C} = \mathbf{E}^{-1}. \tag{B.3}$$

Alternatively, one may subject to nonlocal averaging the inelastic stress $\boldsymbol{\sigma}''$ defined as

$$\boldsymbol{\sigma}'' = \mathbf{E} : \boldsymbol{\epsilon}'' = \mathbf{E} : \boldsymbol{\epsilon} - \boldsymbol{\sigma}(\boldsymbol{\epsilon}), \qquad \bar{\boldsymbol{\sigma}}'' = \int_V \hat{\alpha}(\mathbf{x}, \boldsymbol{\xi}) \boldsymbol{\sigma}''(\boldsymbol{\xi}) \, \mathrm{d}V(\boldsymbol{\xi}). \tag{B.4}$$

The results are of course exactly the same as for the averaging of the inelastic strain.

In this approach, an over-nonlocal formulation is obtained by

$$\boldsymbol{\sigma} = \mathbf{E} : (\boldsymbol{\epsilon} - \hat{\boldsymbol{\epsilon}}), \qquad \hat{\boldsymbol{\epsilon}} = m\bar{\boldsymbol{\epsilon}}'' + (1 - m)\boldsymbol{\epsilon}'', \tag{B.5}$$

where $\hat{\boldsymbol{\epsilon}}$ is the over-nonlocal strain and m is an empirical coefficient, as discussed before.

The replacement of local by nonlocal inelastic strain (Jirásek, 1998) has recently been found to provide only a partial regularization. As pointed out by Jirásek (1998), this kind of nonlocal model leads to nonzero tensile (residual) stresses even at very large displacements across the localization band, which is unrealistic. Therefore, the separation created by an open macroscopic crack cannot be modeled. This classical nonlocal model works well in the peak and early post-peak regions of the effective stress–strain diagrams, but not after the stress gets reduced to less than about one third of the peak stress. This has been proven theoretically (Jirásek, 1998), and numerically documented by the progressive expansion of the fracture process zone. Fig. 20 shows, for the case of a one-dimensional bar, the evolution of the strain profile for different values of m. Increasing the value of coefficient m (Fig. 20a), we see a broadening of the developing localization band. If the value of m is reduced (Fig. 20c), we see a narrowing localization band, but the model still eventually leads at collapse to a fracture process zone spread unrealistically along the entire bar.

It can, however, be shown that, in the one-dimensional case, the only solution with a finite localization zone is that with a constant inelastic strain along the entire bar (an alternative proof of Jirásek, 1998, is given in the following). Considering the case of an infinite bar in which the fracture process zone $\mathscr{F}$ of a nonzero length has developed, the nonlocal inelastic strain, taken from Eqs. (B.2) and (B.3), must be constant and its derivative must vanish:

$$\bar{\epsilon}'' = \epsilon - \frac{\sigma}{E} = \text{constant}, \tag{B.6}$$

$$\frac{\mathrm{d}\bar{\epsilon}''}{\mathrm{d}x} = \int_{-\infty}^{+\infty} \frac{\partial\alpha(r)}{\partial r}\frac{\partial r}{\partial x}\epsilon''(\xi)\,\mathrm{d}\xi = \int_{-\infty}^{+\infty} \frac{\partial\alpha(r)}{\partial r}\operatorname{sgn}(x-\xi)\epsilon''(\xi)\,\mathrm{d}\xi = 0. \tag{B.7}$$

Let us consider point x_0 at the left boundary between the localization zone and the rest of the bar. The integral in expression (B.7) has a positive value, because $\bar{\epsilon}''(x_0) > 0$; $\partial\alpha/\partial r < 0$ for $r < R$ and $\partial\alpha/\partial r = 0$ for $r \geqslant R$; $\operatorname{sgn}(x_0 - \xi) = -1$ for $\xi \geqslant x_0$, and so $\mathrm{d}\bar{\epsilon}''(x_0)/\mathrm{d}x > 0$. This means that Eq. (B.7) is not satisfied; so $\mathrm{d}\bar{\epsilon}''$ cannot be constant in the fracture process band $\mathscr{F}$. Therefore, the only possible solution with a nonzero width of localization band is that with a constant inelastic strain along the bar (in this case $\mathrm{d}\bar{\epsilon}''(x_0)/\mathrm{d}x = 0$ $\forall x_0$). Properly, the inelastic strain must localize into a band of a certain finite width; moreover, the formulation with over-nonlocal inelastic strain, Eq. (B.5), is not able to simulate the deformation process up to the complete loss of cohesion. Even using a refined model with $m > 1$ in this nonlocal formulation with over-nonlocal inelastic strain, Eq. (B.5), still exhibits unrealistic behavior (see Fig. 20).

Analyzing the special case of an infinite uniaxial bar, Planas et al. (1993, 1994) showed that, in the integral nonlocal model with averaging of the inelastic strain, Eq. (B.2), the inelastic strain accepts a solution consisting of a Dirac's δ-function. This makes this nonlocal model in the end physically equivalent to the cohesive crack model.

The over-nonlocal formulation could be adjusted as follows. When fracture propagates, it is intuitive that the interaction between material points across fracture becomes difficult and finally impossible. This behavior could be captured by a nonlocal model with a decreasing characteristic length. Jirásek (1998) proposed combining the nonlocal model with a model for discontinuities embedded in the finite elements, and making the transition when the cracking strain reaches a certain value. This combination is able to correct problems such as spurious shifting of the damage zone when body forces are significant (as in dams) (Jirásek, 1999).

Taking inspiration from this combination, we may assume the coefficient m to be a function of the maximum principal strain. Looking at Eq. (B.5), the linear combination coincides with the nonlocal model for $m = 1$ and with the local model for $m = 0$. The local model may be considered as a nonlocal model with a characteristic length equal to zero. Therefore, reducing m to zero in Eq. (B.5) is equivalent to reducing to zero the characteristic length. The following formula has been considered in computations:

$$m = m_0\left(1 - \frac{(\langle\epsilon_I - \epsilon_I^0\rangle \cdot C)^n}{1 + (\langle\epsilon_I - \epsilon_I^0\rangle \cdot C)^n}\right), \tag{B.8}$$

where m_0 is the initial value for m, ϵ_I^0 is the critical strain value at which the characteristic length starts to decrease, and C and n are two empirical parameters.

One problem connected with this adjustment is that objectivity can be lost when the deformation becomes large. Therefore, the tail of load–displacement curves could be spuriously influenced by mesh refinement.

Appendix C. Numerical implementation

According to the definition of a nonlocal variable, the integral in Eq. (8) over all the volume V of the structure is equal to the sum of the integrals over the individual finite elements. Therefore, the nonlocal variable is computed via Gaussian quadrature, using the same sampling points as those used for integrating the internal force vector of the finite element:

$$f^*(\mathbf{x}) = \sum_{n=1}^{N_e} \sum_{i=1}^{N_g} \alpha(\mathbf{x}, \boldsymbol{\xi}_{ni}) f(\boldsymbol{\xi}_{ni}) W_i \det(J_{ni}), \tag{C.1}$$

$$V_r(\mathbf{x}) = \sum_{n=1}^{N_e} \sum_{i=1}^{N_g} \alpha(\mathbf{x}, \boldsymbol{\xi}_{ni}) W_i \det J_{ni} \quad \text{and} \quad \bar{f}(\mathbf{x}) = \frac{f^*(\mathbf{x})}{V_r(\mathbf{x})}. \tag{C.2}$$

Hence W_i is the weight of integration point i, J_{ni} is the Jacobian of the element n calculated at the integration points i, N_e is the number of elements, N_g is the number of Gaussian integration points per element, and $\boldsymbol{\xi}_{ni}$ are the coordinates of integration points i in element n.

As the computation proceeds, at each integration point, $\mathbf{x}$, one needs the nonlocal quantity, which can be evaluated by the following flowchart:

1. Loop over elements $n = 1, \ldots, N_e$.
   (i) Loop over quadrature points i of the element n.
   (ii) Compute the distance between the current point $\boldsymbol{\xi}_{ni}$ and $\mathbf{x}$. If the distance is greater than R, Eq. (10), go to 2.
   (iii) Compute and sum the contributions to $V_r(\mathbf{x})$ and $f^*(\mathbf{x})$.
   (iv) End of the loop over the quadrature points.
2. End of the loop over the elements.
3. Divide the nonlocal quantity $f^*(\mathbf{x})$ by $V_r(\mathbf{x})$ (Eq. (C.2)).

The nonlocal model in Appendix B is computationally more expensive than that proposed in the main text. In that approach one must first calculate the inelastic strain (Eq. (B.3)), calling the material subroutine for each Gaussian point with a distance less than R (Eq. (10)), and then compute the final stress (Eq. (B.5)) calling the material subroutine.

Two different kinds of solution procedure for nonlinear finite element programs with updated Lagrangian formulation are considered: the explicit solution for transient problems, and the implicit solution for equilibrium problems (Belytschko et al., 2001). Because the microplane model is a three-dimensional constitutive law, a three-dimensional eight-node brick element with 8 integration points is implemented.

An explicit integration in time (based on the central difference method) is adopted. Although it is intended for dynamics, it can be used also for quasi-static problems if the load is applied slowly and proper damping is provided.

A drawback of the explicit time integration is that the time step must be very short because the elements are small, because at least three elements need to fit within the characteristic length (but better more). Another drawback is that solving a quasi-static problem with a dynamic algorithm requires imposing the load very slowly, so as to make the inertial forces negligible.

The equilibrium solution is obtained as the limit of the dynamic solution when the accelerations vanish. The objective of the solution is to make the residuals, corresponding to the out-of-balance forces, vanishingly small. To solve in each loading step the set of nonlinear algebraic equations, the modified version of Newton–Raphson method is used. To avoid the problems due to the lack of positive definiteness of the tangent stiffness matrix in post-peak softening, the initial (elastic) stiffness matrix ($\mathbf{K}$) has been employed in all the computation. In the static problem (with rate-independent material), time t is not the real time but merely a monotonically increasing parameter. The flowchart for the equilibrium analysis is as follows:

1. Initial condition and initialization ($n = 0$, $t = 0$, $\mathbf{d}_{\text{update}} = \mathbf{d}_0$); compute $\mathbf{K}$ and impose the homogeneous displacement boundary conditions. Start a loop on load step.

2. Loop on Newton–Raphson iterations for load increment $n+1$.
3. Compute the internal forces $\mathbf{f}^{\text{int}}(\mathbf{d}, t^{n+1})$ and the residual $\mathbf{r} = \mathbf{f}^{\text{int}}(\mathbf{d}, t^{n+1}) - \mathbf{f}^{\text{ext}}(\mathbf{d}, t^{n+1})$. Solve the linear equations system $\Delta\mathbf{d} = -\mathbf{K}^{-1}\mathbf{r}(\mathbf{d}, t^{n+1})$. Impose the displacement non-homogenous boundary conditions using the penalty method. Update $\mathbf{d} \leftarrow \mathbf{d} + \Delta\mathbf{d}$. Check convergence criterion $\left(\|\Delta\mathbf{d}\|_{l_2} = \left(\sum_{i=1}^{n_{\text{dof}}} \Delta\mathbf{d}_i^2\right)^{1/2} \leqslant \gamma\|\mathbf{d}_{\text{update}} - \mathbf{d}_n\|_{l_2}\right)$ and, if not met, go to 2.
4. Update the displacements, step count and time: $\mathbf{d}^{n+1} \leftarrow \mathbf{d}$, $n \leftarrow n+1$, $t \leftarrow t + \Delta t$.
5. Output. If $t < t_{\max}$ go to 2.

If the initial stiffness matrix is used, the convergence in a highly nonlinear regime is slow. To accelerate the convergence, a modified version of Thomas' acceleration scheme (Sloan et al., 2000) is adopted. The acceleration algorithm consists in rewriting the update displacement, for the ith Newton–Raphson iteration, as follow:

$$\mathbf{d}_i = \mathbf{d}_{i-1} + \alpha_{i-1}\Delta\mathbf{d}_i + \Delta\bar{\mathbf{d}}_i \tag{C.3}$$

where $\Delta\bar{\mathbf{d}}_i = -\mathbf{K}^{-1}\mathbf{r}(\mathbf{d}_{i-1} + \alpha_{i-1}\Delta\mathbf{d}_i, t^{n+1})$. In the first iteration of each time step, we assume $\alpha_0 = 1$, and after that the acceleration factor for the next iteration is obtained by a least-squares fit so that $\alpha_i\Delta\mathbf{d}_i \approx \alpha_{i-1}\Delta\mathbf{d}_i + \Delta\bar{\mathbf{d}}_i$. Solving for α_i we obtain:

$$\alpha_i = \alpha_{i-1} + \frac{\Delta\mathbf{d}_i^{\mathrm{T}} \cdot \Delta\bar{\mathbf{d}}_i}{\Delta\mathbf{d}_i^{\mathrm{T}} \cdot \Delta\mathbf{d}_i}. \tag{C.4}$$

This algorithm needs two back-substitutions and two unbalanced force evaluations for each iteration. It is quite robust and leads to a significant convergence acceleration (Sloan et al., 2000).

The procedure to calculate the internal force is the same for both time integration algorithms. The flowchart is the following:

1. Initialize $\mathbf{f}^{\text{int},n} = \mathbf{0}$.
2. Loop over elements $n = 1, \ldots, N_{\text{e}}$. Initialize $\mathbf{f}_{\text{e}}^{\text{int},n} = \mathbf{0}$.
   (i) Loop over quadrature points $\boldsymbol{\xi}$, $i = 1, \ldots, N_{\text{g}}$. Compute deformation measure, small strains, and the nonlocal quantities according to Eqs. (C.1) and (C.2). Compute stress $\boldsymbol{\sigma}^n(\boldsymbol{\xi})$ by nonlocal microplane model constitutive law and then internal forces contribution $\mathbf{f}_{\text{e}}^{\text{int},n} = \mathbf{f}_{\text{e}}^{\text{int},n} + B^{\mathrm{T}}\boldsymbol{\sigma}^n(\boldsymbol{\xi})\omega(\boldsymbol{\xi})J(\boldsymbol{\xi})$. End loop over quadrature points.
   (ii) Assemble $\mathbf{f}_{\text{e}}^{\text{int},n}$ into the global $\mathbf{f}^{\text{int},n}$. End the loop over elements.

References

Aifantis, E.C., 1984. On the microstructural origin of certain inelastic models. Journal of Engineering Mathematical Technology 106, 326–330.

Bažant, Z.P., 1976. Instability, ductility, and size effect in strain-softening concrete. Journal of Engineering Mechanics Divisions, ASCE 102 (EM2), 331–344, discussions 103, 357–358, 775–777, 104, 501–502.

Bažant, Z.P., 1984. Imbricate continuum and its variational derivation. Journal of Structural Engineering, ASCE 110, 1693–1712.

Bažant, Z.P., 1994. Nonlocal damage theory based on micromechanics of crack interations. Journal of Engineering Mechanics, ASCE 120 (3), 593–617.

Bažant, Z.P., 2004. Scaling theory for quasibrittle structural failure. Proc., National Academy of Sciences 101, in press.

Bažant, Z.P., Belytschko, T., 1985. Wave propagation in strain-softening bar: exact solution. Journal of Structural Engineering, ASCE 111, 381–389.

Bažant, Z.P., Caner, F.C. 2002. Microplane model M5 with kinematic and static constraints for concrete fracture and anelasticity. Report No. 02-12/C699m, Department of Civil Engrg., Northwestern University; Journal of Engineering Mechanics, ASCE, 130, 2004, in press.

Bažant, Z.P., Cedolin, L., 1991. Stability of Structures: Elastic, Inelastic, Fracture and Damage Theory. Oxford University Press, New York.

Bažant, Z.P., Jirásek, M., 2002. Nonlocal integral formulations of plasticity and damage: survey of progress. Journal of Engineering Mechanics, ASCE 128 (11), 1119–1149 (invited ASCE 150th anniversary article).

Bažant, Z.P., Lin, F.-B., 1988a. Nonlocal yield limit degradation. International Journal for Numerical Methods in Engineering 26, 1805–1823.

Bažant, Z.P., Lin, F.B., 1988b. Nonlocal smeared cracking model for concrete fracture. Journal of Structural Engineering, ASCE 114 (11), 2493–2510.

Bažant, Z.P., Lin, F.B., 1989. Stability against localization of softening into ellipsoids and bands: parameter study. International Journal of Solids and Structures 25, 1483–1498.

Bažant, Z.P., Oh, B.-H., 1983. Crack band theory for fracture of concrete. Materials and Structures, RILEM 16 (93), 155–177.

Bažant, Z.P., Oh, B.-H., 1985. Microplane model for progressive fracture of concrete and rock. Journal of Engineering Mechanics, ASCE 111, 559–582.

Bažant, Z.P., Ožbolt, J., 1990. Nonlocal microplane model for fracture, damage and size effect in structures. Journal of Engineering Mechanics, ASCE 116 (11), 2485–2505.

Bažant, Z.P., Prat, P.C., 1988. Microplane model for brittle plastic material: I. Theory; and II. Verification. Journal of Engineering Mechanics, ASCE 114, 1672–1702.

Bažant, Z.P., Pfeiffer, P.A., 1987. Determination of fracture energy from size effect and brittleness number. ACI Materials Journal 1 (84), 463–480.

Bažant, Z.P., Pijaudier-Cabot, G., 1988. Nonlocal continuum damage, localization instability and convergence. ASME Journal of Applied Mechanics 55, 287–293.

Bažant, Z.P., Planas, J., 1998. Fracture and Size Effect in Concrete and Other Quasibrittle Materials. CRC Press, Boca Raton.

Bažant, Z.P., Belytschko, T., Chang, T.-P., 1984. Continuum model for strain softening. Journal of Structural Engineering, ASCE 110, 1666–1692.

Bažant, Z.P., Xiang, Y., Prat, P.C., 1996a. Microplane model for concrete. I. Stress–strain boundaries and finite strain. Journal of Engineering Mechanics, ASCE 122 (3), 245–254.

Bažant, Z.P., Xiang, Y., Adley, M.D., Prat, P.C., Akers, S.A., 1996b. Microplane model for concrete. II. Data delocalization and verification. Journal of Engineering Mechanics, ASCE 122 (3), 255–262.

Bažant, Z.P., Caner, F., Carol, I., Adley, M., Akers, S.A., 2000. Microplane model M4 for concrete. I: formulation with work-conjugate deviatoric stress. Journal of Engineering Mechanics, ASCE 126 (9), 944–953.

Belytschko, T., Liu, W.K., Moran, B., 2001. Nonlinear Finite Elements for Continua and Structures. John Wiley & Sons, Ltd.

Brocca, M., Bažant, Z.P., 2000. Microplane constitutive model and metal plasticity. Applied Mechanics Reviews, ASME 53 (10), 265–281.

Caner, F., Bažant, Z.P., 2000. Microplane model M4 for concrete. II: algorithm and calibration. Journal of Engineering Mechanics, ASCE 126 (9), 954–961.

Caner, F.C., Bažant, Z.P., Červenka, J., 2002. Vertex effect in strain-softening concrete at rotating principal axes. J. Engrg. Mechanics ASCE 128 (1), 24–33.

Carol, I., Bažant, Z.P., 1997. Damage and plasticity in microplane theory. International Journal of Solids and Structures 34 (29), 3807–3835.

Cosserat, E., Cosserat, F., 1909. Théorie des corps déformable. Herman et fils, Paris.

de Borst, R., 1991. Simulation of strain localization: a reappraisal of the Cosserat continuum. Engineering Computation 8, 317–332.

de Borst, R., Mühlhaus, H.B., 1992a. Computational strategies for gradient continuum models with a view to localisation of deformation. In: Bicanic, N., Marovic, P., Owen, D.R.J., Jovic, V., Mihanovic, A. (Eds.), 4th Int. Conf. on Nonlinear Eng. Comp. Pineridge Press, Swansea, pp. 239–260.

de Borst, R., Mühlhaus, H.B., 1992b. Gradient dependent plasticity: formulation and algorithmic aspect. International Journal for Numerical Methods in Engineering 35, 521–539.

di Luzio, G., 2002. A new nonlocal microplane model for fracture and damage of concrete. PhD Thesis, Department of Structural Engineering, Politecnico di Milano.

Eringen, A.C., 1966. A unified theory of thermomechanical materials. International Journal of Engineering Science 4, 179–202.

Jirásek, M., 1998. Nonlocal models for damage and fracture: comparison of approaches. International Journal of Solids and Structures 35, 4133–4145.

Jirásek, M., 1999. Computational aspects of nonlocal models. In: European Conference on Computational Mechanics, Munchen, Germany.

Jirásek, M., Rolshoven, S., 2003. Comparison of integral-type nonlocal plasticity models for strain-softening materials. International Journal of Engineering Science 41, 1553–1602.

Kröner, E., 1968. Elasticity theory of materials with long-range cohesive force. International Journal of Solids and Structures 3, 731–742.

Lasry, D., Belytschko, T., 1988. Localization limiter in transient problem. International Journal of Solids and Structure 24 (6), 581–597.

Loret, B., Prevost, J.H., 1990. Dynamic strain localization in elaso-(visco-)plastic solids, Part 1. General formulation and one-dimensional examples. Computer Methods in Applied Mechanics and Engineering 83, 247–273.

Mühlhaus, H.B., Aifantis, E.C., 1991. A variational principle for gradient plasticity. International Journal of Solids and Structure 28, 845–858.

Mühlhaus, H.-B., Vardoulakis, I., 1987. The thickness of shear band in granular materials. Géotechnique 37, 271–283.

Needleman, A., 1988. Material rate dependence and mesh sensitivity in localization problems. Computer Methods in Applied Mechanics 67, 69–85.

Ožbolt, J., Bažant, Z.P., 1996. Numerical smeared fracture analysis: nonlocal microcrack interaction approach. International Journal for Numerical Methods in Engineering 39, 635–661.

Pamin, J., 1994. Gradient-dependent plasticity in numerical simulation of localization phenomena. PhD Dissertation, TU Delft, Netherlands.

Peerlings, R.H.J., de Borst, R., Brekelmans, W.A.M., de Vree, J.H.P., 1996. Gradient enhanced damage for quasi-brittle materials. International Journal for Numerical Methods in Engineering 39, 3391–3403.

Pijaudier-Cabot, G., Bažant, Z.P., 1987. Nonlocal damage theory. Journal of Engineering Mechanics, ASCE 113, 1512–1533.

Planas, J., Elices, M., Guinea, G.V., 1993. Cohesice crack versus nonlocal model: closing the gap. International Journal of Fracture 63, 173–187.

Planas, J., Elices, M., Guinea, G.V., 1994. Cohesice crack as a solution of a class of nonlocal models. In: Bažant, Z.P., Bittnar, Z., Jirásek, M., Mazars, J. (Eds.), Fracture and Damage of Quasibrittle Structures. E&FN Spon, London, pp. 131–144.

Planas, J., Elices, M., Guinea, G.V., 1996. Basic issue of nonlocal models: uniaxial modeling. Tecnical Report 96-jp03, Departamento de Ciencia de Materiales, ETS de Ingenieros de Caminos. Universidad Politecnica de Madrid, Ciudad Universitaria sn., 28040, Madrid, Spain.

Rolshoven, S., Jirásek, M., 2001. On regularized plasticity models for strain-softening materials. In: de Borst, R. et al. (Eds.), Fracture Mechanics of Concrete Structure. Swets & Zeitlinger, Lisse.

RILEM Committee QFS, 2004. Quasibrittle fracture scaling and size effect. Materials and Structures (Paris) 37, in press.

Saouridis, C., Mazars, J., 1992. Prediction of the failure and size effect in concrete via a bi-scale damage approach. Engineering Computations 9, 329–344.

Schlangen, E., 1993. Experimental and numerical analysis of fracture processes in concrete. PhD Dissertation, TU Delft, Netherland.

Sloan, S.W., Sheng, D.C., Abbo, A.J., 2000. Accelerated initial stiffness schemes for elastoplasticity. International Journal for Numerical and Analytical Methods in Geomechanics 24, 579–599.

Sluys, L.J., 1992. Wave propagation, localization and dispersion in softening solids. PhD Dissertation, TU Delft, Netherland.

Steinmann, P., Willam, C., 1992. Localization within the framework of micropolar of elastoplasticity. In: Mannl, V. et al. (Eds.), Advanced in Continuum Mechanics. Springer Verlag, Berlin, pp. 296–313.

Stroud, A.H., 1971. Approximate Calculation of Multiple Integrals. Prentice-Hall, Englewood Cliffs, NJ.

Strömberg, L., Ristinmaa, M., 1996. FE-formulation of a nonlocal plasticity theory. Computer Methods in Applied Mechanics and Engineering 136, 127–144.

UE Anchor Project, 2001. Anchorages in normal and high performance concretes subjected to medium and high strain rates. Politecnico di Milano, University of Patrass, Hilti Corporation, Densit, JRC-Ispra, Enel-hydro, Bekaert. Final Report, UE ANCHOR Project.

Vardoulakis, I., Aifantis, E.C., 1991. A gradient flow theory of plasticity for granular materials. Acta Mechanica 87, 197–217.

Vermeer, P.A., Brinkgreve, R.B.J., 1994. A new effective non-local strain measure for softening plasticity. In: Chambon, R., Desrues, J., Vardoulakis, I. (Eds.), Localisation and Bifurcation Theory for Soils and Rocks. Balkema, Rotterdam, pp. 89–100.

Zbib, H.M., Aifantis, E.C., 1988. On the localization and postlocalization behavior of plastic deformation, I, II, III. Res Mechanica 23, 261–277, 279–292, 293–305.